Prophage-encoded phage defence proteins with cognate self-immunity

Siân V. Owen[1,2,*], Nicolas Wenner[3,*], Charles L. Dulberger[4, 5], Ella V. Rodwell[3], Arthur Bowers-Barnard[3], Natalia Quinones-Olvera[1,2], Daniel J. Rigden[6], Eric J. Rubin[4], Ethan C. Garner[5], Michael Baym[1,2,†], Jay C. D. Hinton[3,†]

[1] Department of Biomedical Informatics, Harvard Medical School, Boston, MA 02115, USA.
[2] Laboratory of Systems Pharmacology, Harvard Medical School, Boston, MA 02115, USA.
[3] Institute of Infection, Veterinary & Ecological Sciences, University of Liverpool, Liverpool, UK
[4] Department of Immunology and Infectious Diseases, Harvard T. H. Chan School of Public Health, Boston, MA, USA
[5] Department of Molecular and Cellular Biology, Harvard University, Boston, MA, USA
[6] Institute of Systems, Molecular and Integrative Biology, University of Liverpool, UK

Summary

Temperate phages are pervasive in bacterial genomes, existing as vertically-inherited islands called prophages. Prophages are vulnerable to the predation of their host bacterium by exogenous phages. Here we identify BstA, a novel family of prophage-encoded phage defence proteins found in diverse Gram-negative bacteria. BstA drives potent suppression of phage epidemics through abortive infection. The *bstA*-encoding prophage itself is not inhibited by BstA during lytic replication due to a self-immunity mechanism driven by the anti-BstA (*aba*) element, a short stretch of DNA within the *bstA* locus. Phage-targeting by distinct BstA proteins from *Salmonella*, *Klebsiella* and *Escherichia* prophages is functionally interchangeable, but each possesses a cognate *aba* element. The specificity of the *aba* element ensures that immunity is exclusive to the replicating prophage, and cannot be exploited by heterologous BstA-encoding phages. BstA allows prophages to defend their host cells against exogenous phage attack, without sacrificing their own lytic autonomy.

Introduction

The perpetual battle between bacteria and their viruses (phages) has driven the evolution of a diverse array of phage defence systems in bacteria (Bernheim and Sorek, 2020; Hampton et al., 2020; Houte et al., 2016; Rostøl and Marraffini, 2019. Conversely, it is increasingly recognised that phages have evolved many mechanisms to subvert these defence systems (Maxwell, 2017; Samson et al., 2013; Trasanidou et al., 2019). Though perhaps the most intuitive form of phage defence involves the direct rescue of an infected cell, for example by the targeted degradation of phage nucleic acids by CRISPR-Cas, or restriction modification systems, many phage-defence systems in fact function solely at the population level. In a mechanism conceptually analogous to the pathogen-stimulated programmed cell death driven by the innate immune systems of higher organisms (Abedon, 2012), population-level defence systems prevent phage infection spreading across entire populations, at the cost of the lives of infected cells.

Population-level phage defence systems are often grouped under the umbrella term “abortive infection” (Abi) (Labrie et al., 2010; Lopatina et al., 2020) and represent diverse mechanisms to prevent phage replication and cause cell death. These include protease-mediated inhibition of cellular translation (Bingham et al., 2000), toxin-antitoxin pairs (Fineran et al., 2009) and cyclic oligonucleotide signalling (Cohen et al., 2019). Recently, it has been proposed that certain CRISPR-Cas systems function through abortive infection (Meeske et al., 2019; Watson et al., 2019). Such mechanistic diversity and prevalence of abortive infection systems in bacteria underscores the selective advantage this strategy imparts in the battle against phages.

However, an important sub-plot in the bacteria-phage conflict is the pervasive existence of so-called “temperate” or “lysogenic” phages *within* bacterial genomes. Temperate phages are able to stably exist within the bacterial chromosome as latent, vertically inherited islands known as a prophages. Crucially, to find new hosts, prophages must escape from the bacterial genome and return to the lytic life-cycle (spontaneously, or in response to specific molecular cues). The prophage-state imposes unique existential pressures, wherein the fitness of the phage is indefinitely tied to that of the bacterium.

Indirectly enhancing their own fitness, prophages frequently encode “moron” or “accessory” loci that modulate the biology of host bacteria (Bondy-Denomy and Davidson, 2014; Fortier and Sekulovic, 2013; Howard-Varona et al., 2017) in a phenomenon likened to altruism (Shub, 1994). Prophage accessory loci are frequently associated with bacterial pathogenesis, and many notorious bacterial pathogens depend on prophage-encoded toxins and virulence factors to cause disease (Brüssow et al., 2004; Fortier and Sekulovic, 2013). However, another trait conferred by prophages that can significantly increase bacterial fitness, is resistance against bacteriophage attack. Indeed, recent work has shown that prophage accessory genes may represent an underexplored reservoir of phage-defence systems (Bondy-Denomy and Davidson, 2014; Dedrick et al., 2017; Snyder, 1995).

Here, we report a novel phage defence system driven by the BstA protein and encoded by prophages of diverse Gram-negative bacteria. When a bacterium harbours a *bstA*-encoding prophage, BstA protein confers effective population-level phage defence through abortive infection. The *bstA* locus includes an anti-BstA element, which can suppress the activity of BstA protein to allow the native prophage to undergo lytic replication. We propose that such elegant molecular systems have evolved to allow prophages to defend their host cells from predatory phages, without compromising their own potential for lytic replication.

Results

The BTP1 prophage-encoded *bstA* gene mediates phage resistance

Salmonella enterica subsp. *enterica* serovar Typhimurium (*S.* Typhimurium) strain D23580 encodes the ~40 kb prophage BTP1 (Figure 1A) (Owen et al., 2017). An operon within BTP1, the *gtr* locus ($gtrAC^{BTP1}$), has been shown to confer resistance against phage P22 due to chemical modification of the cellular lipopolysaccharide (LPS), which is the receptor for phage P22 (Kintz et al., 2015). Unsurprisingly therefore, we found deleting the BTP1 prophage from strain D23580 (D23580 ∆BTP1) made the strain highly susceptible to infection by phage P22, confirming that resistance to phage P22 is conferred by the BTP1 prophage (Figure 1B). However, inactivation of the *gtr* locus of prophage BTP1 (D23580 $\Delta tsp\text{-}gtrAC^{BTP1}$) did not restore sensitivity to phage P22 to the level of D23580 ∆BTP1 (Figure 1B), suggesting a second phage resistance system existed on this prophage. Our previous transcriptomic study showed that the *bstA* gene was highly-expressed during lysogeny, and therefore a candidate for modulation of the biology of the *S.* Typhimurium cell (Owen et al., 2020). The *bstA* gene, encoded downstream of the prophage repressor locus, has been implicated in both virulence, and anti-virulence, of *Salmonella* isolates, but no functional mechanism has been proposed (Herrero-Fresno et al., 2014, 2018; Spiegelhauer et al., 2020). We hypothesised that *bstA* was the second element in the BTP1 prophage that conferred defence against phage P22.

Consistent with this hypothesis, removal of the *bstA* gene from prophage BTP1 (D23580 ∆*bstA*), did dramatically increase susceptibility to phage P22. To confirm that phage resistance was directly mediated by BstA protein, we introduced two stop codons into the beginning of the *bstA* coding sequence by exchanging 4 nucleotides (D23580 $bstA^{STOP}$) (Figure 1B). D23580 $bstA^{STOP}$ was highly susceptible to P22 phage, to the same level as D23580 ∆*bstA*, demonstrating that BstA protein mediates defence against phage P22. Simultaneous deletion of the *gtr* locus and inactivation of the BstA protein (D23580 $\Delta tsp\text{-}gtrAC^{BTP1}\ bstA^{STOP}$) fully recapitulated the susceptibility to phage P22 achieved by deleting the entire BTP1 prophage (D23580 ∆BTP1), indicating that resistance to phage P22 is solely mediated by the *bstA* and *gtr* loci in prophage BTP1. We reproduced these findings by replicating phage P22 in liquid culture, demonstrating that reduction of plaque formation by BstA truly reflected phage replication suppression (Supplementary Figure 1A).

To investigate whether the function of the BstA protein depended on other elements on the BTP1 prophage, we constructed an inducible expression system in *S.* Typhimurium strain LT2. LT2 is the type strain of *S.* Typhimurium, and is natively susceptible to many phages, including P22. Expression of the $BstA^{BTP1}$ protein in *S.* Typhimurium LT2 from within a neutral position on the chromosome (LT2 $tetR\text{-}P_{tetA}\text{-}bstA$) conferred a high degree of resistance to P22 and other phages including ES18 and 9NA (Figure 1C; Supplementary Figure 1B). Expression of the derivative containing two stop codons at the beginning of the *bstA* coding sequence ($bstA^{STOP}$) did not confer any phage resistance, demonstrating

again that the effect is mediated by BstA protein (Supplementary Figure 1C). However, BstA did not mediate resistance against all phages tested: Det7, Felix O1, and notably, phage BTP1 (which encodes the *bstA* gene) were unaffected by expression of BstA, both at the level of plaque assay and replication in liquid culture (Figure 1C; Supplementary Figure 1B). We could not detect any pattern in the characteristics of phages that were sensitive or insensitive to BstA protein that could relate the mechanistic action of BstA protein.

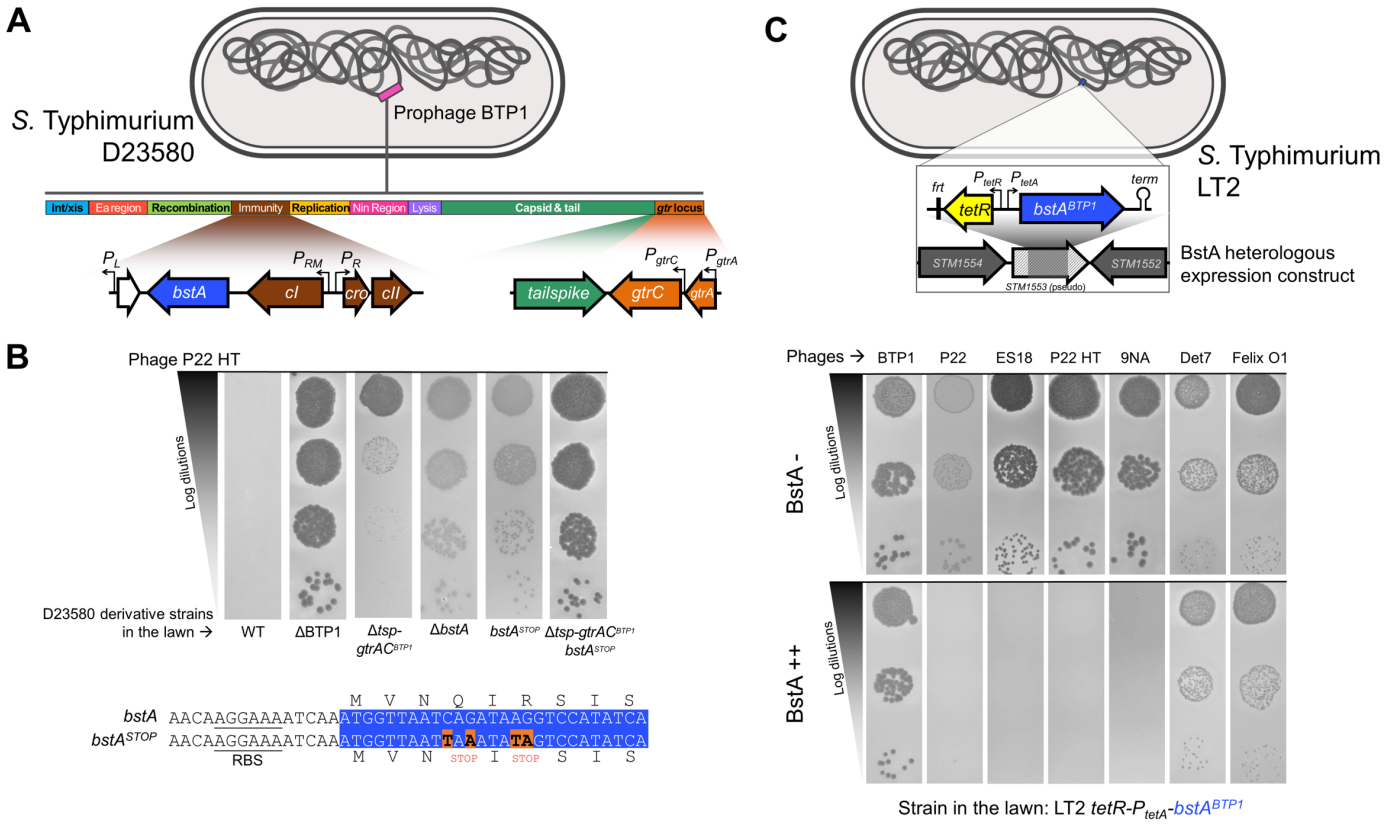

Figure 1: The *bstA* gene of prophage BTP1 confers phage defence
(**A**) Genomic architecture of prophage BTP1 of *S.* Typhimurium D23580, according to Owen *et al.,* 2020: the LPS modification genes $gtrAC^{BTP1}$ (Kintz et al., 2015) and the immunity region carrying *bstA* (downstream of the *cI* repressor gene) are detailed. Bent arrows represent promoters. (**B**) Removal of prophage BTP1 from strain D23580 results in enhanced sensitivity to phage P22. Two BTP1 genes confer resistance to P22; *gtrAC* and *bstA*. Plaque assays were performed with phage P22 HT *105/1 int-201* (P22 HT) applied to lawns of *S.* Typhimurium D23580 WT or ΔBTP1, Δ*bstA*, $bstA^{STOP}$, $\Delta tsp\text{-}gtrAC^{BTP1}$ and $\Delta tsp\text{-}gtrAC^{BTP1}$ $bstA^{STOP}$ mutants (strains JH3877, SSO-204, SSO-78, JH4287 and SNW431, respectively). The requirement for the inactivation of *tsp* is describes in the Methods. The 4 SNPs leading to two nonsense mutations in the $bstA^{STOP}$ strain are indicated. RBS: putative ribosome binding site. The *bstA* open reading frame is highlighted in blue. (**C**) BstA protein confers phage defence in *S.* Typhimurium LT2. Phages P22, ES18, P22HT and 9NA are inhibited by BstA. Phages Det7, Felix O1 and BTP1 are not affected by BstA expression. Plaque assays were carried out with the indicated *Salmonella* phages applied to lawns of LT2 $tetR\text{-}P_{tetA}\text{-}bstA^{BTP1}$ (JH4400) in the absence (BstA-) or the presence of the inducer anhydrotetracycline (AHT, BstA++). The $tetR\text{-}P_{tetA}\text{-}bstA$ insertion replacing a part of the *STM1553* pseudogene of strain JH4400 is schematized above: *tetR* encodes the tetracycline repressor that represses the P_{tetA} promoter in the absence of AHT induction, "*frt*" denotes the 84 nt scare sequence of pKD4 and the hairpin represents the native *bstA* Rho-independent terminator (*term*).

BstA represents a novel family of prophage-encoded phage defence proteins in diverse Gram-negative bacteria

Having established that BstA functions as a prophage-encoded phage defence system, we sought to further characterise the occurrence of this protein in bacteria. We found BstA protein homologs in the genomes of diverse Gram-negative bacteria (Supplementary Table 1) and we compiled a dataset of 72 homologs representative of phylogenetic diversity. The majority (79%) of these BstA homologs co-occurred with phage genes, and therefore were designated as putatively-prophage associated (Figure 2A). No known phage-associated genes were found in the vicinity of 21% (15 of 72) of BstA homologs, which were considered to be putatively prophage-independent. A small subset of BstA homologs were plasmid-encoded, and this group included both putatively prophage-associated and -independent homologs (Figure 2A). Strikingly, in many cases, BstA homologs were located downstream of putative prophage repressor proteins, mirroring the genetic architecture of $BstA^{BTP1}$ (Figure 2B). The BstA protein appears to be highly associated with prophages of Gram-negative bacteria.

Whilst the BstA protein does not exhibit sequence homology to any functionally-characterised proteins, remote homology detection methods revealed a putative KilA-N domain in the N-terminal region (residues 32-147 of $BstA^{BTP1}$)) (Figure 2C). Though poorly characterised, the KilA-N domain is found in proteins from phages and eukaryotic DNA viruses, and contains the helix-turn-helix motif characteristic of DNA binding proteins (Iyer et al., 2002; Medina et al., 2019). A large screen based on genomic proximity to known-phage defence systems previously predicted KilA-N domain containing proteins to play a role in phage defence (Doron et al., 2008). The KilA-N domain derives its name from the *kilA* gene product of bacteriophage P1 (lethal when expressed in *E. coli*) but *kilA* has no known function in phage infection biology (Hansen, 1989), and no bacterial KilA-N domain-containing proteins have been functionally characterised to date.

Certain residues in the BstA protein are highly conserved amongst homologs from diverse members of the Alpha-, Beta-, and Gamma- Proteobacteria (Figure 2C; Supplementary Figure 2). A small number of BstA protein homologs (all found in Cyanobacterial plasmids) only exhibited homology to the N-terminal, putative KilA-N domain. A second small group corresponding to Proteobacteria, Cyanobacteria and a single Bacteroidetes isolate were only homologous to the C-terminal region of BstA (shown at the bottom on the alignment in Figure 2C). Such bipartite protein homology suggests that the BstA protein is composed of two functional domains. Additionally, we observed that the identity of BstA protein homologs did not obviously correlate with bacterial taxonomy. For example, homologs from enteric bacteria closely-related to *Salmonella* (members of the Gammaproteobacteria) sometimes shared less identity to $BstA^{BTP1}$ than homologs from alpha- and betaproteobacteria, suggesting BstA proteins are frequently horizontally transferred, perhaps consistent with their association with prophages.

We selected two diverse BstA homologs from *Klebsiella pneumoniae* (48.4% amino acid identity to $BstA^{BTP1}$) and *E. coli* (41.7% identity) to investigate the phage-resistance function of the larger BstA protein family (the native genetic context of these homologs is illustrated in Figure 2B, and their identity to $BstA^{BTP1}$ is highlighted in the alignment in Figure 2C). We engineered inducible expression systems for the BstA the expression construct we previously validated for $BstA^{BTP1}$ (Figure 3A,B; Figure 1C). Expression of $BstA^{Kp}$ and $BstA^{Ec}$ in *S.* Typhimurium LT2 conferred resistance to *Salmonella* phages at a similar level to $BstA^{BTP1}$, despite these homologs only sharing around 40% identity at the amino acid level (Figure 3A,B; Supplementary Figure 3A). Importantly, $BstA^{Kp}$ and $BstA^{Ec}$ showed additional activity against phage BTP1 (which encodes $bstA^{BTP1}$), a property that was not shown by $BstA^{BTP1.}$

Finally, to investigate the phage-defence function of BstA against well-characterised coliphages, we expressed $BstA^{BTP1}$ and $BstA^{Ec}$ in *E. coli*. Heterologous expression of $BstA^{BTP1}$ in *E. coli* strain MG1655 conferred resistance to phage λ, ϕ80, P1 and T7, but did not affect phages T4 and T5 (Supplementary Figure 3B,C). Surprisingly we found $BstA^{Ec}$ was slightly less active against coliphages than $BstA^{BTP1}$ (Supplementary Figure 3B,C). We note that replication in liquid culture is a more reliable and reproducible measure of phage susceptibility than plaque assay, and we frequently observed stronger resistance phenotypes liquid replication than by plaque assay (Supplementary Figure 3B,C).

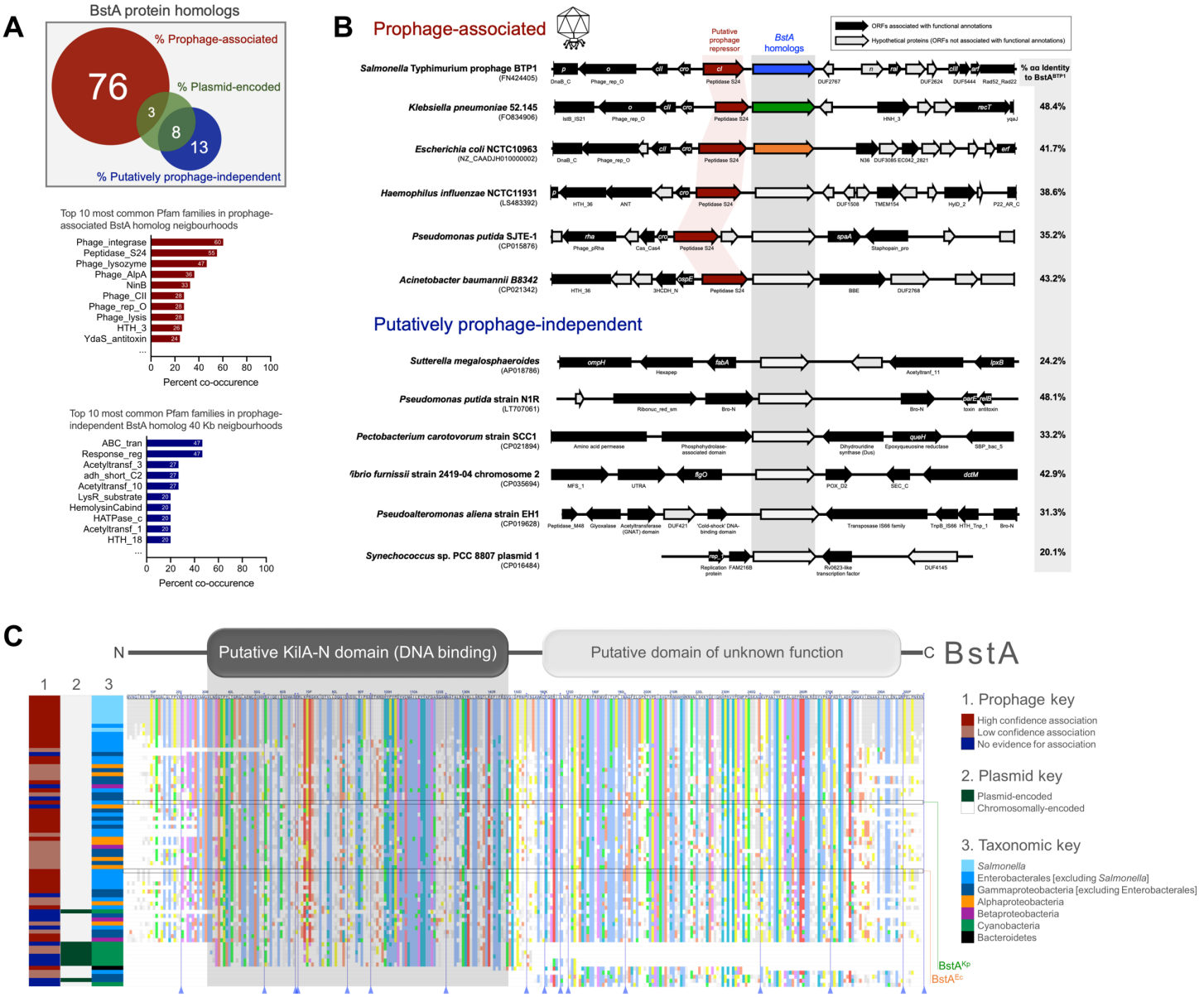

Figure 2: BstA homologs are found in diverse bacterial taxa and are frequently associated with prophages
(**A**) A dataset of 72 BstA homologs representative of taxonomic diversity were manually curated and analyzed for prophage association based on the co-occurrence of phage-related Pfam-domains in the 20 kb either side of each homologs (yielding a total 40 kb window) (Supplementary Table 2). Homologs without co-occurring phage-related protein domains were assigned as "Putatively prophage-independent". A further subset of the BstA homologs were encoded on plasmids. The top ten most commonly co-occurring Pfam domains with prophage-associated and putatively prophage-independent BstA homologs are shown as bar graphs. (**B**) Gene maps showing the genetic context of prophage-associated and putatively prophage-independent BstA homologs. Putative prophage repressor genes are highlighted in red. The top three BstA proteins from BTP1 ($BstA^{BTP1}$, blue), *K. pneumoniae* 52.145 ($BstA^{Kp}$, green) and *E. coli* NCTC10963 ($BstA^{Ec}$, orange) are studied experimentally in later stages of this work, and are highlighted. Open reading frames associated with functional annotations are shown as solid black arrows, and functional gene name or Pfam domains are annotated. (**C**) An alignment of the 72 BstA protein homologs to $BstA^{BTP1}$, with colors indicating amino acid conservation. Alignment columns containing gaps relative to the reference sequence ($BstA^{BTP1}$) have been collapsed and are indicated with blue lines and triangles at the base of the alignment (an expanded alignment can be found in Supplementary Figure 2). The position of $BstA^{Kp}$ and $BstA^{Ec}$ within the alignment is highlighted. The position of the putative KilA-N domain ($BstA^{BTP1}$ residues 32-147) is indicated by a grey box. Heatmaps on the left of the alignment indicate the prophage and plasmid association of each homolog (lanes 1 & 2), and the taxonomic group each homolog derives from (lane 3). Prophage association was split into high and low confidence based on gene co-occurrence criteria (see Methods).

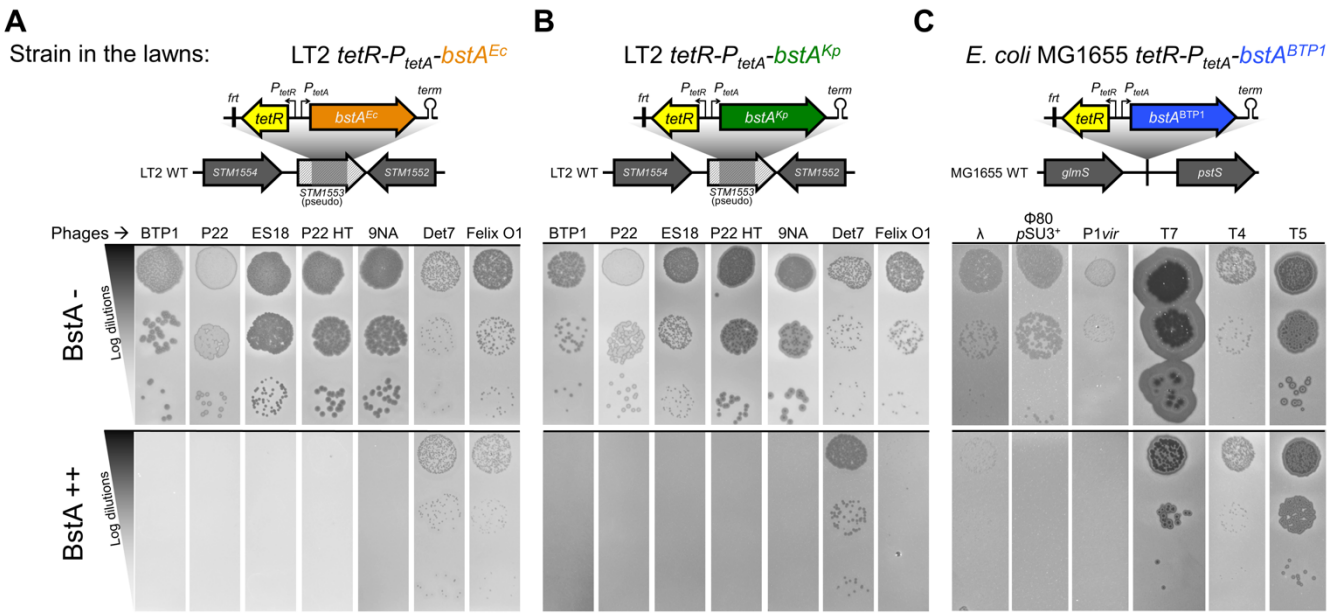

Figure 3: BstA homologs from *Salmonella, E. coli* and *K. pneumoniae* all confer phage defence
Heterologous expression of *bstA* homologues from (**A**) *E. coli* NCTC10963 ($bstA^{Ec}$) and (**B**) *K. pneumoniae* Kp52.145 ($bstA^{Kp}$) in *Salmonella* strain LT2 confers phage defence at similar levels to $bstA^{BTP1}$, but show additional activity against phage BTP1. (**C**) $BstA^{BTP1}$ confers defence against coliphages in *E. coli* MG1655. Plaque assays were carried out with the indicated phages applied on mock-induced (BstA-) or AHT-induced (BstA++) lawns of LT2 *tetR-*P_{tetA}*-*$bstA^{Ec}$ (JH4408), LT2 *tetR-*P_{tetA}*-*$bstA^{Kp}$ (JH4404) or MG1655 *tetR-*P_{tetA}*-*$bstA^{BTP1}$ (JH4410). The *tetR-*P_{tetA}*-bstA* insertions in LT2 or in the *glmS-pstS* intergenic of MG1655 are depicted above.

We conclude that BstA represents a novel family of phage-resistance proteins associated with prophages in diverse Gram-negative bacteria.

BstA mediates effective population-level phage defence through abortive infection

Phage resistance systems function *via* diverse functional mechanisms (Hampton et al., 2020; Rostøl and Marraffini, 2019). We used a microscopy-based approach to understand how BstA mediates phage-resistance. P22 phages were used to infect *Salmonella* cells with and without native $BstA^{BTP1}$ function, at high multiplicity of infection (MOI) in order to ensure that most cells were infected. We were surprised to observe that independent of $BstA^{BTP1}$ function, all cells lysed within the time course of 3 hours (Figure 4A, Supplementary Video 1), and $BstA^{BTP1}$ function did not appear to confer any direct protection from phage infection. We conducted the same experiment in liquid culture, measuring phage replication and the fraction of surviving cells *post* phage infection. In cells possessing functional BstA (D23580 Δ*tsp-gtrAC*), phage P22 Δ*c2* completely failed to replicate (Figure 4B). In contrast, in the absence of BstA function (D23580 Δ*tsp-gtrAC* $bstA^{STOP}$), the phage replicated >100-fold. However, despite preventing the replication of phage P22, $BstA^{BTP1}$ had no effect on cell survival: independent of $BstA^{BTP1}$ function only 1-2% of cells survived (Figure 4C). We hypothesised that BstA protein must instead mediate phage defence at the population level.

To investigate whether BstA protein mediated population-level phage defence, we conducted a second microscopy experiment, wherein approximately only 1 in every 1000 cells was infected with phage P22. Unlike during liquid culture, in our microscopy setup cells were immobilised on agarose pads, which restricts the movement of phage particles to local diffusion. Using this setup, we tracked the spread of infection as primary infected cells lysed and produced secondary infections. To facilitate tracking of phage replication, we used a reporter phage engineered to encode the red fluorescent protein mCherry within the early lytic operon (P22Δ*c2 p-mCherry*), so that fluorescence signal indicated phage replication (Figure 4D).

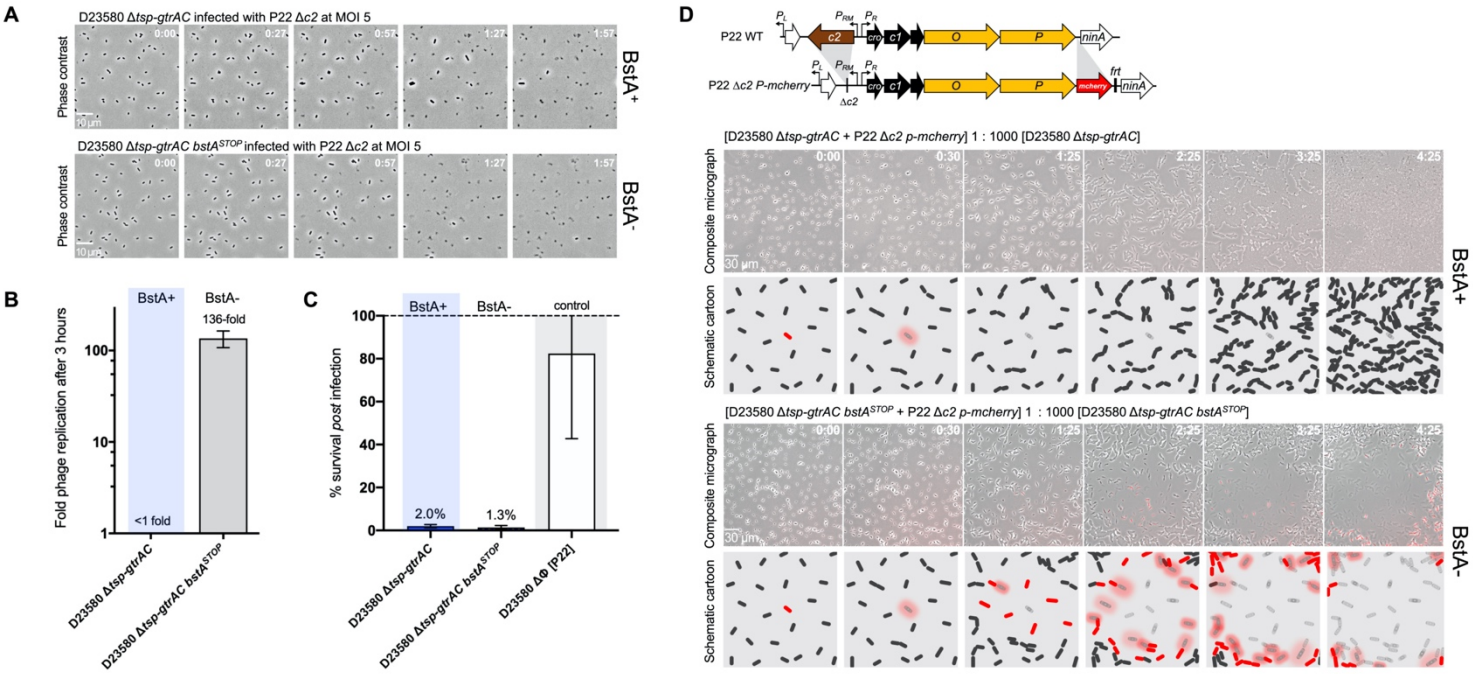

Figure 4: BstA mediates population-level phage defence through abortive infection
BstA protein does not protect individual cells from phage infection. (**A**) Cells natively expressing BstA [D23580 Δ*tsp-gtrAC*, JH4287] or possessing a mutated BstA locus [D23580 Δ*tsp-gtrAC bstA*^{STOP}, SNW431] were infected with the obligately virulent P22-derivate phage, P22Δ*c2*, at an MOI of 5 to increase the likelihood of infecting all cells. Infected cells were imaged on agarose pads and the images represent a time series. Regardless of BstA function, almost all cells were observed to lyse (indicated by loss of defined cell shape and phase contrast). Videos of the time series are presented in Supplementary Video 1. (**B**) A phage replication assay showed that P22Δ*c2* phage failed to replicate after three hours growth on the BstA+ strain [D23580 Δ*tsp-gtrAC*], but replicated ~136-fold when BstA was inactivated [D23580 Δ*tsp-gtrAC bstA*^{STOP}]. (**C**) Survival assay of the same strains after infection by phage P22Δ*c2*, at an MOI of 5. Consistent with the microscopy data in (A), BstA function did not affect cell survival from phage infection. D23580 ΔΦ [P22] (SSO-128), a phage P22 lysogen (and therefore natively resistant), was used as a negative control. (**D**) A fluorescent reporter module for phage replication was added to P22Δ*c2* (P22Δ*c2 p-mcherry*) so that phage replication yielded red fluorescence *(mcherry* was inserted into the lytic genes of the phage). A similar experiment to (A) was conducted, but P22Δ*c2 p-mcherry* infected cells were mixed 1:1000 with uninfected cells. In the BstA+ cells, primary infected cells lysed, but did not stimulate secondary infections of neighbouring cells, and eventually formed a confluent lawn. In BstA- cells, primary lysis events caused secondary infections (neighbouring cells showing red fluorescence and subsequent lysis) causing an epidemic of phage infection reminiscent of plaque formation. Cartoon**s** schematise the outcomes of these experiments in the two strain backgrounds. Videos of the time series are presented in Supplementary Video 2.

In the population lacking functional BstA^{BTP1} (D23580 Δ*tsp-gtrAC bstA*^{STOP}), primary infected cells lysed after around 30 minutes (Figure 4D, Supplementary Video 2). Subsequently, the red fluorescence signal was observed in neighbouring cells revealing secondary infection, followed by cell lysis, a cycle which repeated until all cells in the radius of the primary infected cell had lysed, reminiscent of plaque formation (Figure 4C). The impact of the epidemic of phage infection upon bacterial cells lacking BstA^{BTP1} can be seen clearly in Supplementary Video 2.

In contrast, in the population with native BstA activity (D23580 Δ*tsp-gtrAC*) no fluorescence signal or lysis was observed in neighbouring cells following the lysis of the primary infected cells. Instead, neighbouring cells continued to grow, eventually forming a confluent lawn (Figure 4D, Supplementary Video 2). The lack of subsequent rounds of secondary infection after the primary cell lysis events indicates that viable phage were not released upon cell lysis. Furthermore,

Taken together, these experiments demonstrate that BstA protein inhibits successful phage replication, but does not prevent the death of the infected cell. BstA therefore provides phage defence at the population-level and prevents the spread of phage epidemics. We propose that BstA is a novel abortive infection system: a population-level phage defence system that inhibits phage infection at the cost of cell viability.

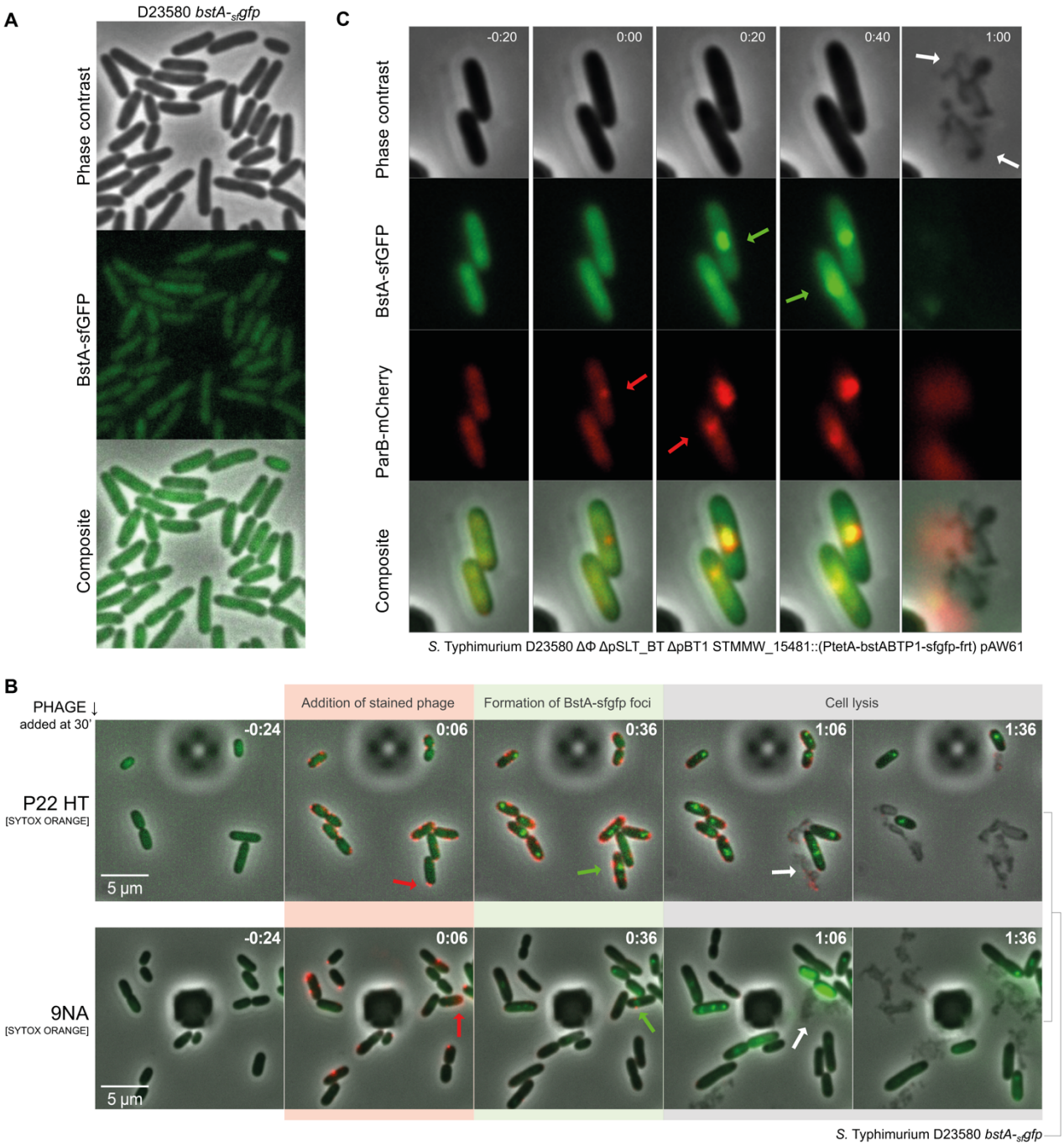

Figure 5: BstA protein responds dynamically to phage infection and colocalises with phage DNA
(**A**) A translational fusion of BstA protein to $_{sf}$GFP protein (D23580 *bstA-$_{sf}$gfp,* SNW403) was constructed to track the location of BstA protein inside cells. In the absence of phage infection, GFP signal is diffuse within the cell cytoplasm, suggesting no specific sub-cellular localisation. (**B**) A microfluidic growth chamber was used to observe the behaviour of BstA protein during phage infection, capturing images every 1.5 minutes. A time series of representative fields are presented as composite images (phage contrast, green and red fluorescence are overlaid). Cells were first grown for a period in the chamber (immobilised by the angle of the chamber ceiling) with constant flow of M9 Glu+ media (Methods). Fluorescently labelled phages P22 HT or 9NA (stained with SYTOX Orange resuspended in M9 Glu+ media , Methods) were then added to the cells, and can be seen adsorping to cells as red fluorescent puncta (red arrows). For purposes of comparison, timestamps are synchronised to the point at which phage are first observed. Typically around 20 minutes after initial observation of phage infection, BstA proteins formed discrete and dynamic foci within the cells (green arrows). Cells then proceeded to lyse (white arrows), consistent with previous microscopy data in Figure 4. Videos of the time series are presented in Supplementary Video **3**. (**C**) A microfluidic growth chamber was used to co-localise BstA protein and the DNA of infection phage. SVO251 cells (expressing the BstA-$_{sf}$GFP fusion and a ParB-mCherry fusion protein**)** were grown for a period of 15 minutes before P22 Δ*pid::parS-aph* phages were flowed across the cells. The ParB-mCherry fusion protein oligomerises at the *parS* site on the infecting phage DNA, so that mCherry foci indicate the subcellular location of phage DNA (red arrows). For the purposed of comparison, the time stamp was set to zero at the first observation of mCherry foci (i.e. the earliest detectable event of phage infection). BstA foci formed directly after appearance of mCherry foci (green arrows), and merging of the images (composite) shows that the foci are overlapping, indicating that BstA foci correspond to infecting phage DNA. Cells proceeded to lyse (white arrows). Videos of the time series are presented in Supplementary Video 4.

291 **BstA protein responds dynamically to phage infection and co-localises with phage DNA**
292
293 To explore the molecular activity of BstA during phage infection, we constructed a translational fusion
294 of the BstA^{BTP1} protein to superfolder green fluorescent protein ($_{sf}$GFP), confirming that the translational
295 fusion did not compromise the function of the BstA protein (Supplementary Figure S4). We used time-
296 lapse fluorescence microscopy to observe the dynamics of BstA protein inside individual cells during
297 infection with two phages P22 and 9NA. In the absence of phage infection, BstA protein was distributed
298 diffusely within the cytoplasm of the cells, suggesting no particular sub-cellular localisation (Figure 5A,
299 Supplementary Video 3). However, approximately 20 minutes after infection with phages P22 and 9NA,
300 we consistently observed BstA protein aggregating into discrete foci towards the centre of infected cells
301 (Figure 5B, Supplementary Video 3). Cell lysis occurred approximately 40 minutes after the formation
302 of BstA foci.
303
304 We speculated that the dynamic establishment of foci by BstA in response to phage infection was likely
305 to reflect the mechanistic activity of the BstA protein. We noticed that the dynamics of the foci formed
306 by BstA proteins during phage infection were reminiscent of live-cell fluorescence microscopy studies
307 of phage replisomes (Cenens et al., 2013; Trinh et al., 2017). We therefore speculated that the focus of
308 BstA protein in phage infected cells might correspond to the replicating phage DNA. To test this
309 hypothesis, we used a ParB-*parS* system to track the sub-cellular localisation of phage DNA relative to
310 BstA protein. We inserted a *parS* site into the P22 phage chromosome, and expressed a ParB-mCherry
311 fusion protein inside cells already expressing BstA-$_{sf}$GFP. ParB protein oligomerises onto DNA at *parS*
312 sites, and therefore *parS*-tagged DNA is indicated by ParB-mCherry foci. We conducted a microfluidic
313 infection experiment to co-locate BstA foci and infecting P22 phage DNA, and we observed that the
314 position of ParB-mCherry foci (corresponding to phage P22 DNA) clearly overlapped with foci formed
315 by BstA-$_{sf}$GFP (Figure 5C, Supplementary Video 4). The microscopy data suggest that BstA protein
316 interacts with the replicating DNA of infecting phages.
317
318 Together the data are consistent with a model where BstA proteins are titrated to sites of phage
319 replication inside infected cells, to suppress the successful multiplication of the phage.
320
321 **BstA phage resistance systems contain anti-BstA elements (*aba*) that suppress the activity of**
322 **BstA**
323
324 When characterising the sensitivity of different phages to the activity of BstA^{BTP1} using our heterologous
325 expression system (Figure 1C), we observed that BTP1 phage, (which itself encodes the *bstA^{BTP1}* gene)
326 was not affected by expression of BstA^{BTP1} (schematised in Figure 6A). We hypothesized that BTP1
327 carries an anti-BstA determinant: a self-immunity factor that allows phage BTP1 to replicate without
328 being targeted by its own abortive infection protein. Consistent with this hypothesis, phage BTP1
329 became sensitive to BstA^{BTP1} expression when the *bstA* coding sequence was deleted (BTP1 Δ*bstA*).
330 (Figure 6B). The self-immunity function of the *bstA* locus was not affected by the introduction of the
331 double stop codon mutation into the beginning of the coding sequence (as described in Figure 1B),
332 indicating that self-immunity is not mediated by the BstA protein itself, but by an alternative genetic
333 element encoded within the *bstA* locus (Figure 6B). Here, and for the duration of this report, we define
334 the *bstA* "locus" as the region including the *bstA* coding sequence and the 5' upstream sequence.
335
336 To identify the precise genetic basis of BstA self-immunity, we constructed a library of BTP1 mutant
337 phages, carrying truncations of different lengths from the 3' end of the *bstA* locus (Supplementary Figure
338 5A) and screened these phages for their ability to replicate in the presence of BstA^{BTP1} expression. Self-
339 immunity was preserved in all the mutant phages (i.e. insensitivity to BstA^{BTP1} expression) except the
340 mutant with the largest *bstA* truncation (BTP1 *bstA$^{\Delta 24}$*), in which just the first 24 bp of the *bstA* reading
341 frame were intact (Supplementary Figure 5A). A similar truncation mutant containing just the first 34 bp
342 of *bstA* (BTP1 *bstA$^{\Delta 34}$*) retained immunity to BstA, indicating that the anti-BstA determinant was encoded
343 within the upstream region and first 34 bp of the *bstA* gene. Consistently, the transfer of *bstA$^{\Delta 34}$* (the first
344 34 bp of *bstA,* including the upstream sequence) to phage P22 (P22 *bstA$^{\Delta 34I}$*), conferred BstA immunity
345 (Supplementary Figure 5B). To identify the minimal sequence required for BstA self-immunity, we
346 constructed further P22 *bstA$^{\Delta 34I}$*-derived phages, successively truncating the transferred sequence from
347 the 5' end (P22 *bstA$^{\Delta 34I}$* - P22 *bstA$^{\Delta 34V}$*, Supplementary Figure 5B). We discovered that a 63 bp sequence

(GCCCGCCACACTTTAACAAGGAAAATCAAATGGTTAATCAGATAAGGTCCATATCACCCCGCC) spanning 29 bp of the upstream region and the first 34 bp of *bstA* (start codon underlined) was necessary and sufficient to confer the self-immunity (Figure 6C). We designated this 63 bp element '*aba*', for anti-BstA. Supplying the 63 bp *aba* sequence on the high-copy number pUC18 plasmid (pUC18-*aba*) rescued P22 phage replication in the presence of BstA protein, demonstrating that the self-immunity function of *aba* functions in *trans* (Supplementary Figure 6A).

The *aba* element is DNA-based

In the native BTP1 prophage, the *aba* sequence overlaps the start of the *bstA* gene, preventing the mutational disruption of the *aba* element without modifying the BstA protein sequence. We therefore used the simple multi-copy plasmid *trans*-complementation system (wherein the BstA protein and the *aba* sequence are independently encoded) to further probe the function of the *aba* sequence (Supplementary Figures 6A). A notable feature of the 63 bp *aba* sequence is the presence of a direct "CCCGCC" repeat at the terminal ends, which we hypothesised might be functionally important. Single nucleotide exchange of the CCCGCC→CCCTCC in the first (aba^{mut1}) and second (aba^{mut2}) repeat abolished the self-immunity function of the *aba* element on the phage and *in trans* (Supplementary Figure 6B) showing that the *aba* terminal direct repeats are important for the *aba*-BstA interaction.

The *aba* plasmid *trans*-complementation system additionally allowed us to interrogate the genetic nature of the *aba* element, which we hypothesised could be either DNA, RNA transcript or peptide-based. Though three short open reading frames exist within the *aba* sequence, (Supplementary Figure 6C), non-synonymous mutations of the reading frames did not ablate *aba* function, suggesting the *aba*-driven immunity is not mediated by a short peptide. Secondly, we tested whether transcription of *aba* was necessary for immunity. The *aba* sequence was cloned in either orientation into the *Salmonella* chromosome, downstream of the arabinose-inducible P_{BAD} promoter (D23580 ΔΦ *tetR-bstA*^{BTP1} P_{BAD}-*aba;* Supplementary Figure 6D) to produce high levels of *aba* RNA transcripts. High-level transcription of *aba* RNA did not restore P22 or 9NA plaque formation in the presence of BstA protein, suggesting transcription of *aba* is not required for anti-BstA activity. However, this experiment also demonstrated that supplying *aba* as a single copy on the chromosome also did not confer self-immunity (Supplementary Figure 6D), suggesting that *aba* can only suppress BstA protein when it is encoded on high-copy replicative elements. Further mutational disruption of the *aba* sequence revealed that the self-immunity function was not robust to mutation at multiple sites in the 63 bp sequence (Supplementary Figure 6E). Collectively, our data suggest that *aba*-driven suppression of BstA is neither peptide or transcript mediated, and instead support a model where BstA suppression is mediated by *aba* DNA in *trans*, perhaps by a copy-number dependent mechanism.

The *aba* element prevents the *bstA*-encoding prophage from aborting its own lytic replication

A unique feature of the BstA system, unusual amongst the majority of mechanistically-characterised abortive infection systems, is its frequent occurrence on prophages (latent forms of active phages) (Figure 2A). Prophages must be able to switch to lytic replication, or else the prophage-state becomes an evolutionary dead-end for the phage. It follows therefore, that prophages must be obligately immune to any self-encoded phage-defence systems. Despite this intuitive assumption, self-immunity functions in prophage-encoded phage defence systems have not been previously identified.

We hypothesised that the primary biological role of the *aba* element is to allow the endogenous *bstA*-encoding phage to escape BstA-mediated inhibition upon induction from the prophage-state. To test this, we measured the level of induction of prophage P22 in the presence of heterologously expressed BstA^{BTP1} protein (Figure 6D). In the absence of BstA^{BTP1}, the P22 prophage generated a titer of ~$4x10^9$ PFU/mL after 5 hours growth with inducing agent (mitomycin C, MitC). However, with BstA^{BTP1} expression, the MitC-induced titer of P22 dropped >300-fold to ~$1x10^7$ PFU/mL, consistent with BstA-mediated inhibition of P22 phage replication. Transfer of the *aba* sequence to prophage P22 (P22 *aba*) significantly increased the induced titer in the presence of BstA^{BTP1} to ~$3x10^9$, restoring it to the level seen in the absence of BstA, showing that the *aba* element rescues phage replication *via* suppression of BstA.

Consistent with our hypothesis, we found the *aba*^{mut1} mutation (exchange of a single functionally important nucleotide in the terminal direct repeat) reduced the MitC-induced titer of phage BTP1 ~14-fold in the presence of BstA. This reduction was rescued by supplying the functional *aba* sequence *in trans* on the pUC18 plasmid (Figure 6E), confirming that the *aba*^{mut1} mutation ablates the function of the *aba* element.

These intricate experiments demonstrate that an *aba* element is required for the *bstA*-encoding prophage to switch from lysogenic to lytic replication. In the absence of *aba,* the *bstA*-encoding prophage suffers replication inhibition by its own BstA protein (self-targeting), presumably by the same abortive infection mechanism that inhibits exogenous phage infection.

Possession of a functional *aba* element, which specifically suppresses BstA activity during prophage replication (perhaps *via* a copy-number dependent mechanism), is required to allow the prophage to protect its host from phage infection during lysogeny, whilst permitting its own lytic replication upon induction.

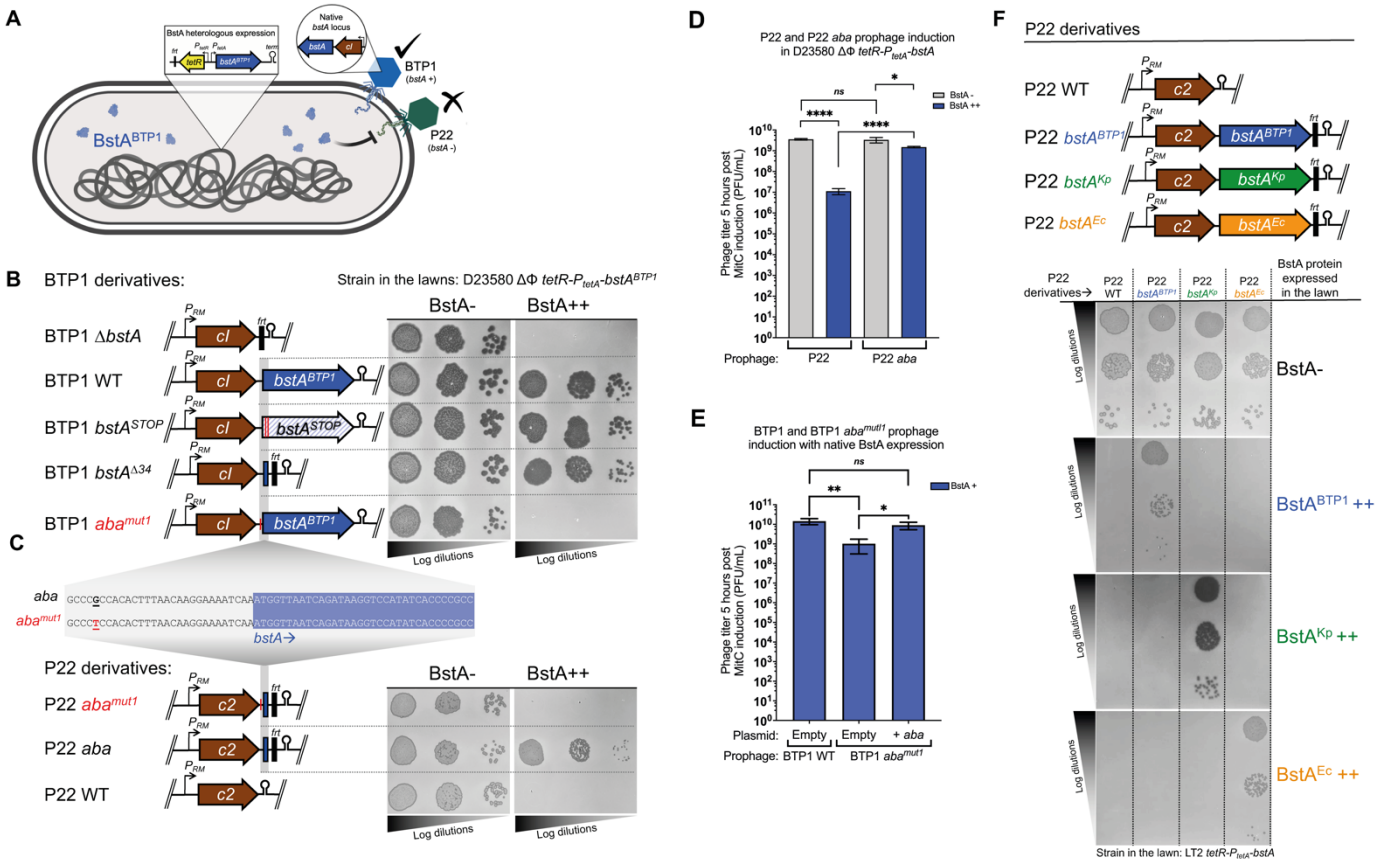

Figure 6: BstA systems include cognate self-immunity elements, *aba*, which are required for successful prophage induction

(**A**) Cartoon summarising the data from Figure 1C. The BTP1 phage, which encodes the *bstA* locus, is not affected by heterologous expression of BstA^{BTP1}. (**B**) Schematic of the BTP1-derived phages used. (**C**) Schematic of the BTP1-derived phages used. In all cases, introduced sequences (*bstA* homologs or fragments) were inserted downstream of the *c2* repressor gene of P22 and are linked to the *frt* sequence. Hairpins represent rho-independent terminators. Insensitivity of the BTP1 phage to BstA^{BTP1} is dependent on the *bstA* locus on the phage chromosome. However, only the first 34 bp of the *bstA* locus are required. The *aba* sequence in P22 and BTP1 counteracts the BstA-driven phage resistance and the G→T mutation (*aba*^{mu1}) suppresses the anti-*bstA* interference. Plaque assays presented in panels B & C were carried out with the indicated phages, applied on mock-induced (BstA-) or AHT-induced (BstA++) lawns of the indicated strain (strains JH4400, JH4404 and JH4408 for panel B, SNW576 for panel C). (**D**) BstA represses P22 prophage induction in the absence of *aba*. P22 induction was measured in D23580 ΔΦ *tetR-P*$_{tetA}$*-bstA*^{BTP1} lysogenized with prophages P22 WT or P22 *aba* (strain SNW583 and SNW585, respectively). Induction was measured 4 hours post AHT-induction (BstA++) or mock-induction (BstA-). (**E**) Endogenous *bstA* of BTP1 represses prophage induction in the presence of the *aba*^{mut1} mutation. Prophage spontaneous induction was measured in strain D23580 ΔΦ ΔTn*21* (Ap^{S}) lysogenized with BTP1 WT (*aba*^{WT}) or BTP1 *aba*^{mut1} (strain SNW597 and SNW598, respectively). Lysogens were transformed with pUC18 (vector) or pUC18-*aba* (pNAW203, +*aba*) and prophage induction was measured 5 hours post induction with Mitomycin C. Data E & F are presented as the mean of biological triplicates ± SD. Groups were compared using unpaired two-tailed Student *t*-test and P values and significance are indicated by *,**,***,**** or ns (not significant). (**F**) Each *bstA* locus encodes a homolog-specific anti-*bstA* element (*aba*) that suppresses BstA-mediated phage defence. Transfer of each *bstA* locus to phage P22 confers immunity against the cognate BstA protein only.

440 **Distinct BstA proteins are associated with cognate *aba* elements**
441
442 Finally, we determined whether the *aba* sequence from $bstA^{BTP1}$ could suppress the activity of the BstA
443 proteins of other bacteria. We challenged the P22 $bstA^{BTP1}$ phage (immune to expression of $BstA^{BTP1}$
444 due to the presence of *aba*) against expression of $BstA^{Ec}$ or $BstA^{Kp}$. The $bstA^{BTP1}$ locus did not protect
445 P22 from the heterologous BstA proteins, indicating that each BstA protein has a cognate *aba* element
446 (Figure 6F). To further test this hypothesis, we engineered P22 phages to encode either $bstA^{Ec}$ or $bstA^{Kp}$
447 (including the respective upstream sequence). Consistent with a cognate BstA-*aba* interaction, P22
448 $bstA^{Ec}$ became specifically immune to expression of $BstA^{Ec}$; and P22 $bstA^{Kp}$ gained specific immunity to
449 $BstA^{Kp}$ expression (Figure 6F). Each *bstA* locus therefore encodes highly-specific self-immunity. We
450 conclude that though BstA proteins are broadly functionally interchangeable in terms of phage-defence
451 activity, each *bstA* locus contains a cognate *aba* element, inactive against heterologous BstA proteins.
452 The specificity of the *aba* self-immunity element means that heterologous *bstA*-encoding phages cannot
453 bypass BstA-mediated abortive infection, and *aba*-mediated suppression of BstA is exclusive to the
454 induced prophage.
455
456 **BstA protein inhibits the replication of phage DNA**
457
458 Sequence-based analysis of BstA protein homologs suggested that the N-terminal domain may bind
459 DNA (Figure 2C), and fluorescence microscopy showed BstA protein interacting with phage DNA. The
460 replication of DNA is a crucial for phage morphogenesis, as new copies of the phage chromosome are
461 required for packaging into capsids. To test whether BstA protein inhibits phage DNA replication in a
462 manner that can be suppressed by *aba*, we conducted Southern blot experiments to monitor levels of
463 phage DNA during infection. Using our prophage-negative, inducible BstA-expression strain (D23580
464 ΔΦ $tetR\text{-}P_{tetA}\text{-}bstA^{BTP1}$), we first tested the replication of the BstA-sensitive virulent phage, 9NA. In the
465 absence of BstA expression, the level of phage 9NA DNA gradually increased over a 50 minute infection
466 time course, indicating successful phage replication (Figure 7A). No accumulation of phage 9NA DNA
467 was observed in the presence of $BstA^{BTP1}$, suggesting that BstA protein strongly inhibited the replication
468 of phage DNA.
469
470 Consistent with the self-immunity function of *aba*, BTP1 phage DNA replication was not affected by the
471 expression of $BstA^{BTP1}$, unless the *aba* element was non-functional (BTP1 aba^{mut1}) (Figure 7B). Likewise,
472 successful replication of phage P22 DNA in the presence of $BstA^{BTP1}$ only occurred when the phage
473 possessed a functional *aba* element (Figure 6B).
474
475 To confirm that BstA protein inhibits DNA replication, we constructed small phage-derived plasmids
476 ('phagemids') based on the phage P22 replication module (Figure 7C). P22 phagemid derivatives that
477 included the functional 63 bp *aba* sequence (pP22-*aba*), or the non-functional aba^{mut1} sequence (pP22-
478 aba^{mut1}) were made.
479
480 The P22 phagemids were transformed into *Salmonella* cells in the presence or absence of $BstA^{BTP1}$
481 protein expression. In the absence of BstA, the stable replication of all three P22 phagemids in
482 *Salmonella* cells generated $>10^6$ transformants /ng phagemid. However, expression of $BstA^{BTP1}$ reduced
483 the transformation efficiency of pP22 (lacking the *aba* sequence) to around 10^1 transformants /ng.
484 Addition of the *aba* sequence to the phagemid (pP22-*aba*) restored the transformation efficiency of the
485 phagemid in the presence of BstA to BstA-negative levels.
486
487 We conclude that phage DNA replication is strongly suppressed by BstA, but replication can be rescued
488 by the *aba* element, presumably by inhibition of BstA protein. As replicated phage DNA is an essential
489 substrate for packaging into phage capsids, the inhibition of DNA replication is likely to prevent the
490 production of infectious progeny phages. We propose that BstA blocks phage replication by inhibiting
491 DNA replication, a process that can be suppressed by the native prophage with the *aba* self-immunity
492 element.

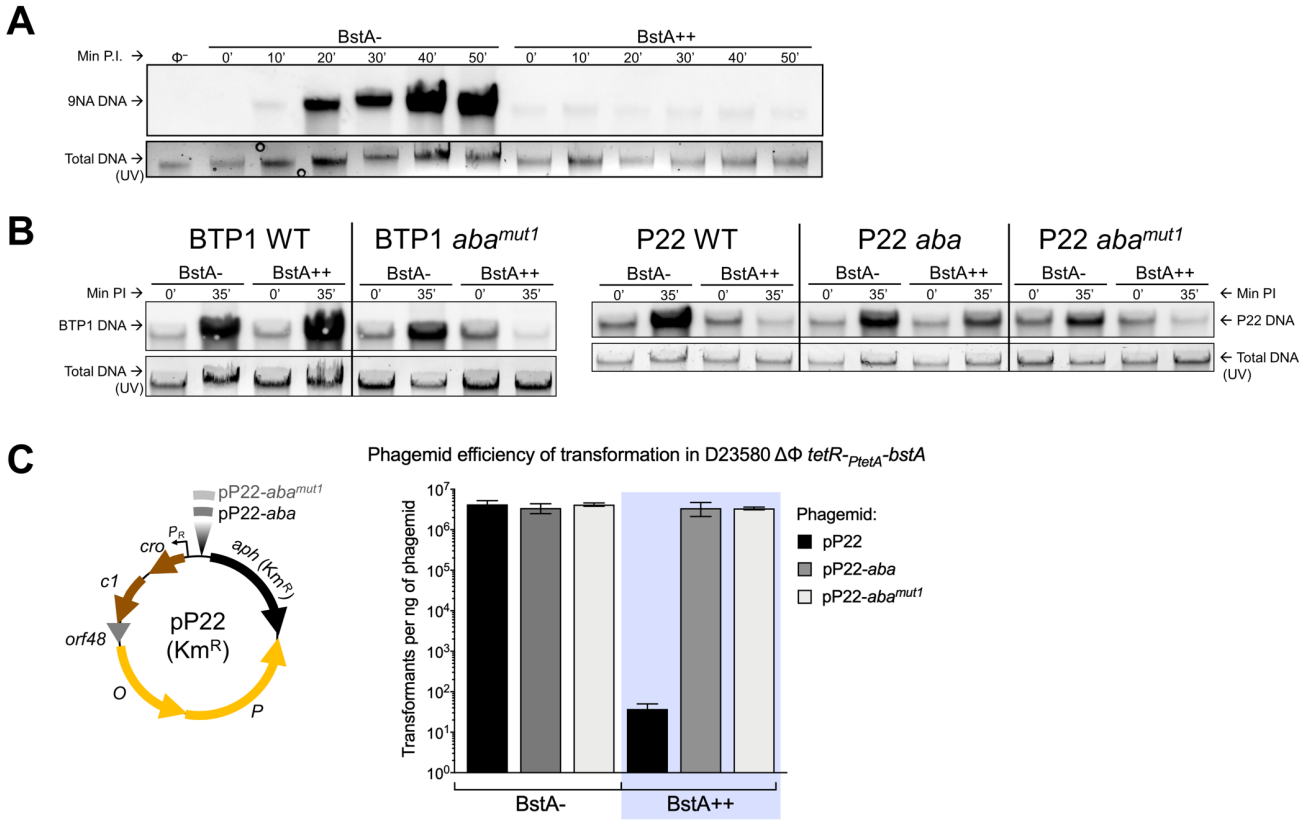

Figure 7: BstA protein inhibits phage DNA replication in the absence of *aba*
DNA replication of 9NA phage (**A**), BTP1 and P22-derived phages (**B**) in the absence or presence of BstA expression. Phage DNA was detected by Southern blotting with total DNA extracted from mock-induced (BstA-) or AHT-induced (BstA++) host strain D23580 ΔΦ *tetR-P*$_{tetA}$*-bstA*^{BTP1} (SNW576), infected by the indicated phage at M.O.I.=5. Before the transfer procedures, total stained DNA was visualized from gels under UV light and the resulting pictures served as loading control. Min PI = minutes post infection. Non-infected SNW576 DNA was used as negative control to check the DNA probe specificity. (**C**) *aba* dramatically increases the transformation efficiency of P22 derived phagemids in BstA expressing *Salmonella*. The Km^R phagemids pP22 (pNAW229), pP22-aba (pNAW230) and P22-*aba*^{mut1} (pNAW231) are schematized and the efficiency of transformation for each phagemid was measured in Mock- or AHT-induced competent bacteria of strain D23580 ΔΦ *tetR-P*$_{tetA}$*-bstA*^{BTP1} (SNW576). Data are presented as the mean of biological triplicates ± SD.

Discussion

Prophages (latent phages residing within the genomes of bacteria) frequently encode accessory genes that bestow beneficial functions on their host bacteria (Bondy-Denomy and Davidson, 2014). A function that can significantly increase bacterial fitness in many environments is phage resistance, and prophages may represent a large reservoir of uncharacterised phage defence systems (Dedrick et al., 2017; Snyder, 1995).

Here, we have discovered a novel family of prophage-encoded abortive infection proteins (BstA) which efficiently defend bacterial populations from phage epidemics. BstA protein is constitutively expressed inside cells that carry the prophage, and provides effective population-level phage defence through abortive infection, inhibiting phage replication at the cost of the viability of individual infected cells. Possession of such innate phage defence systems by active prophages imposes an obvious challenge: the prophage must avoid self-targeting by its own defence system when switching to lytic replication.

We realised that the native prophage which encodes BstA required a mechanism to counteract the protein upon induction from the prophage-state, to avoid aborting its own lytic replication. The BstA

523 system solves this problem with the *aba* element (anti-BstA), a co-encoded short DNA sequence that
524 specifically suppresses the activity of BstA protein upon prophage induction, giving the induced
525 prophage self-immunity to BstA. Theoretically, such a system might leave BstA-expressing cells
526 vulnerable to infection by heterologous BstA-encoding phages, which could use their own *aba* element
527 to bypass native BstA. This problem is avoided by each BstA protein being suppressed only by its
528 cognate *aba* element, ensuring that BstA supression is specific to the native BstA-encoding prophage.
529
530 Despite having been studied for over 60 years, abortive infection systems remain mysterious, and very
531 few have been characterised more deeply than the level of broad functional mechanism (Labrie et al.,
532 2010). Here, we present a complete high-level picture of the BstA phage defence system, and the
533 corresponding anti-BstA *aba* element. We are left with two major questions regarding the BstA protein.
534 Firstly, what are the phage determinants for BstA sensitivity? Though BstA was active against
535 approximately 50% of the phages tested, we did not to detect similarities between BstA-targeted and
536 non-targeted phages that could reflect the molecular determinants of sensitivity. It remains possible that
537 rather than responding to a physical phage stimulus, such as phage DNA or protein, BstA protein
538 responds to a cellular stimulus produced by the infection of specific types of phages.
539
540 Secondly, what is the precise molecular mechanism by which BstA protein inhibits phage DNA
541 replication? Our data show that phage DNA does not replicate in the presence of BstA. The existence
542 of a putative DNA-binding domain in BstA proteins, and microscopic observation of BstA co-localisation
543 with phage DNA makes it tempting to speculate that BstA interacts physically with phage DNA, for
544 example by occlusion of a replication initiation site. In the well-characterised phages P22 and Lambda,
545 DNA replication initially occurs bi-directionally from the origin of replication, generating circular θ-form
546 intermediates (Weigel and Seitz, 2006). These circular forms act as templates for subsequent rolling-
547 circle replication, generating the long concatemeric phage chromosomes needed as the substrate for
548 the packaging machinery of most tailed phages (Fujisawa and Morita, 1997). We speculate that the
549 timing of BstA focus formation, approximately 20 minutes after phage infection, is consistent with the
550 formation of circular θ-form phage DNA. It is possible that BstA specifically inhibits the switch to rolling
551 circle DNA replication, thereby limiting the availability of linear phage chromosomes for packaging into
552 progeny phage capsids. Such a mechanism has been proposed to explain how phage satellites are able
553 to block replication of the ICP1 phage in *Vibrio cholerae* (Barth et al., 2020). Furthermore, numerous
554 Abi systems in *Lactococcus* have been proposed to interfere with phage DNA replicative functions
555 (Chopin et al., 2005), though the molecular mechanisms have not been characterised.
556
557 Alongside the mechanistic details of the BstA protein that have yet to be established, little is known
558 about the interaction of BstA with the *aba* element. Our data show that *aba* interacts with BstA in DNA
559 form, but the mechanism by which *aba* DNA suppresses BstA protein is unclear. Our data indicate that
560 multiple copies of the *aba* element can suppress BstA protein activity in *trans*, which could explain why
561 *aba* function is specific to prophage induction (when prophage DNA is replicated to a high copy number).
562 Further study of the BstA-*aba* system is required to resolve the precise molecular mechanisms by which
563 BstA-encoding prophages, such as BTP1, achieve self-immunity.
564
565 We consistently observed that phage-infected cells underwent cell lysis independent of the activity of
566 BstA protein. However we cannot be certain whether BstA protein causes cell lysis actively or passively.
567 Abi systems have frequently been termed “altruistic suicide” systems, which mediate “programmed cell
568 death” in response to phage infection (Abedon, 2012; Shub, 1994). Whilst perhaps a useful conceptual
569 analogy for the strictly population-level effect of Abi systems, this narrative implies that Abi systems
570 actively cause cell death. Though this is likely to sometimes be the case, such as in the CBASS system
571 (Cohen et al., 2019) or toxin anti-toxin based systems (Fineran et al., 2009), Abi can also be achieved
572 by simple disruption of the phage replication pathway. Because phage lysis is generally a temporally
573 programmed event that occurs independently of successful virion morphogenesis (Cahill & Young,
574 2018), phage-mediated cell lysis can occur in the absence of virion assembly. For example many
575 *Lactococcus* Abi target aspects of phage replication, such as AbiZ, which may interact with phage holin
576 proteins, to stimulate premature cell-lysis before virion assembly is completed (Durmaz and
577 Klaenhammer, 2007).
578

It is possible that BstA protein simply inhibits infectious phage particle formation, for example by precluding the formation of concatemeric DNA for packaging, whilst allowing the phage lysis pathway to proceed unperturbed. As we did not observe a difference in the timing of cell lysis for phage infected cells in the presence or absence of BstA during microscopy studies, we prefer a model where the BstA protein allows the phage lytic pathway to proceed as normal to cell lysis, except that infectious progeny phage particles are not released.

An intriguing feature of the BstA phage defence system is its tight association with prophages, and specifically, with the prophage repressor locus. Though we found homologs in diverse Gram-negative bacteria, the genetic architecture of the *bstA* locus (i.e. lying downstream of, and presumably sharing the promoter of the prophage repressor) was strikingly conserved. The region between the repressor (*cI*) and *n* gene of lambdoid phages has previously been identified as a hotspot of mosaic diversity (Degnan et al., 2007). In fact, the corresponding site in phage Lambda harbours the *rexAB* genes, perhaps the most widely studied prophage-encoded abortive infection system (Snyder, 1995). Despite >60 years of research, the molecular mechanisms governing RexAB activity are poorly understood. RexB is reported to be an ion channel, which triggers loss of cell membrane potential upon activation by the intracellular sensor RexA (Labrie et al., 2010; Snyder, 1995). Whilst not mechanistically comparable to BstA, perhaps the shared synteny of the BstA and RexAB abortive infection systems points to a functional significance of this genomic region, as the *cI* repressor gene is one of the most highly transcribed prophage promoters during lysogeny.

Though somewhat functionally analogous to toxin-antitoxin systems, to our knowledge no other example of self-immunity mechanisms have been described within prophage-encoded abortive infection systems. However there is some evidence supporting the widespread existence of such mechanisms. For example, it was observed that the activity of Lambda RexB protein can be suppressed by overexpression of the *rexB* gene relative to *rexA.* It was speculated, but not shown experimentally, that high levels of RexB might allow phage Lambda to replicate lytically in the presence of RexAB (Parma et al., 1992) i.e. giving the Lambda prophage self-immunity against its own Abi proteins. Our discovery of the BstA and the *aba* element strongly supports this hypothesis.

The discovery of the BstA-*aba* system opens unexplored avenues of research into the mechanisms used by prophages to suppress their own phage-defence activities. We anticipate that similar strategies may be widespread and commonplace, perhaps existing within characterised prophage-encoded phage defence systems. Given the huge mosaic diversity of temperate phages, and high prevalence of uncharacterised accessory genes, the reservoir of prophage-encoded phage defence and self-immunity systems is likely vast and largely unexplored.

615 **Methods**
616
617 **RESOURCE AVAILABILITY**
618 Further information and requests for bacterial and bacteriophage strains should be addressed to the
619 Lead Contact.
620
621 **EXPERIMENTAL MODEL AND SUBJECT DETAILS**
622 **Bacteria and bacteriophages**
623 The full list of bacterial strains used and constructed is available in Supplementary Table 2. All the
624 *Salmonella* strains were derived from the African *S.* Typhimurium strain D23580 (GenBank:
625 FN424405.1) (Kingsley et al., 2009) or the model *S.* Typhimurium strain LT2 (GenBank:
626 AE006468.2)(McClelland et al., 2001; Zinder and Lederberg, 1952). All the *Escherichia coli* strains
627 constructed were derived from *E. coli* strain K-12 substrain MG1655 (GenBank: NC_000913.3) (Riley
628 et al., 2006). The *bstA* homologs were cloned from *E. coli* NCTC10963 (GenBank:
629 NZ_CAADJH010000002.1) or from *Klebsiella pneumoniae* Kp52.145 (GenBank: FO834906.1) (Bialek-
630 Davenet et al., 2014). Bacteriophages (phages), including the temperate phages P22 (GenBank:
631 NC_002371.2) (Pedulla et al., 2003) and BTP1 (GenBank; NC_042346.1) (Owen et al., 2017) and their
632 derivatives, are described in Supplementary Table 2. The genomic coordinates and gene identifiers
633 indicated below refer to the GenBank accession numbers mentioned above.
634
635 **METHOD DETAILS**
636 **Growth conditions and transformation**
637 All suppliers of chemical and reagents are specified in the Key Resources Table. Unless stated
638 otherwise, bacteria were grown at 37°C in autoclaved Lennox Broth (LB: 10 g/L Bacto Tryptone, 5 g/L
639 Bacto Yeast Extract, 5 g/L NaCl) with aeration (shaking 220 rpm) or on LB agar plates, solidified with
640 1.5% Agar. The salt-free LBO media contained 10 g/L Bacto Tryptone, 5 g/L Bacto Yeast Extract. Pre-
641 cultures were inoculated with isolated colonies from agar plates and grown to stationary phase (for at
642 least 6 hours) in 5 mL LB in 30 mL universal glass tubes or in 50 mL plastic tubes (Greiner).
643
644 Cultures were typically prepared by diluting the pre-cultures [1:100] or [1:1000] in LB, and bacteria were
645 grown in conical flasks containing 10% of their capacity of medium (*i.e.* 25 mL LB in a 250 mL conical
646 flask) with aeration. For fluorescent microscopy experiments, bacteria were grown in M9 minimal
647 medium (Sambrook and Russell, 2001) supplemented with 0.4% glucose and 0.1% Bacto Casamino
648 Acids Technical (M9 Glu^+).
649
650 When required, antibiotics were added to the media: 50 µg/mL kanamycin monosulfate (Km), 100 µg/mL
651 Ampicillin sodium (Ap), 25 µg/mL tetracycline hydrochloride (Tc), 20 µg/mL gentamicin sulfate (Gm), 20
652 µg/mL chloramphenicol (Cm). Bacteria carrying inducible constructs with genes under the control of the
653 P_{BAD} or P_m promoters were induced by adding 0.2 % (w/v) L-(+)-arabinose or 1 mM *m*-toluate,
654 respectively. For the strains carrying *tetR*-P_{tetA} modules, P_{tetA} induction was triggered by adding 500
655 ng/mL of anhydrotetracycline hydrochloride (AHT, stock solubilized in methanol). For these constructs,
656 the same volume of methanol was added to the non-induced cultures (mock treatment). Chemically-
657 competent *E. coli* were prepared with RbCl-based solutions and were transformed by heat shock (Green
658 and Rogers, 2014).
659
660 For the preparation of electro-competent cells, bacteria were grown in the salt-free medium LBO to an
661 Optical Density at 600 nm (OD_{600}) of 0.4-0.5. The bacteria were washed twice with cold sterile Milli-Q
662 water (same volume as the culture volume) and were concentrated 100 times in cold 10% glycerol, prior
663 to storage at -80°C. When ultra-competent *Salmonella* cells were required, the bacteria were grown in
664 LBO at 45°C to OD_{600} 0.4-0.5, because growth at high temperature inactivates the *Salmonella* restriction
665 systems (Edwards et al., 1999). Competent cells (10-50 µL) were mixed with 10-5000 ng of DNA in
666 electroporation cuvettes (2 mm gap) and the reactions were electroporated (2.5 kV) using a MicroPulser
667 electroporator (Bio-Rad). Bacteria were re-suspended in 0.5-1 mL LB and incubated for recovery at
668 37°C (30°C for temperature sensitive plasmids) with aeration, for at least one hour. Finally, the
669 transformed bacteria were spread on selective LB agar plates and transformant colonies were obtained
670 after at least 12 hours incubation at 30-37°C.
671

672 **Cloning procedures**
673 All the plasmids and DNA oligonucleotides (primers) are listed in Supplementary Table 2. DNA
674 manipulation and cloning procedures were carried out according to the enzyme and kit supplier
675 recommendations and to standard procedures (Sambrook and Russell, 2001). DNA purity and
676 concentration were measured with a DeNovix DS-11 FX spectrophotometer/fluorometer and using the
677 Qubit dsDNA HS assay Kit.
678
679 For all the cloning procedures, Polymerase Chain Reactions (PCRs) were performed with the Phusion
680 High Fidelity DNA polymerase, purified template DNA and primers in the presence of 3 % Dimethyl
681 Sulfoxide and 1 M betaine, when required. Prior to Sanger sequencing of the constructs, PCR reactions
682 were carried out directly from bacteria or phages with MyTaq Red Mix 2X. PCR fragments were analysed
683 by electrophoresis, purified and finally sequenced with the appropriate primers (Lightrun service,
684 Eurofins Genomics) (Supplementary Table 2).
685
686 All the plasmids were constructed as detailed in the Supplementary Table 2 and were verified by Sanger
687 sequencing. Insertions of DNA fragments into plasmids were performed by digestion/ligation
688 procedures, using restrictions enzymes and the T4 DNA ligase. In addition, PCR-driven restriction-free
689 cloning techniques were used: overlap extension PCRs (Heckman and Pease, 2007) and plasmid
690 assembly by PCR cloning (Van Den Ent and Löwe, 2006) were performed with chimeric primers, purified
691 template DNA and Phusion DNA polymerase, as described previously (Owen et al., 2020). Cloning
692 reactions were transformed by heat shock into *E. coli* Top10 (Invitrogen) or S17-1 *λpir* (Simon et al.,
693 1983). New template plasmids were constructed to insert fluorescent protein encoding genes into
694 *Salmonella* or *E. coli* chromosomes, as reported previously (Gerlach et al., 2007). These plasmids carry
695 the *ori*R6K γ origin of replication of pEMG, the *frt-aph-frt* (Km^R) module of pKD4 linked to gfp^+ (pNAW52),
696 $_{sf}$*gfp* (encoding for superfolder GFP, pNAW62) or *mcherry* (pNAW73), amplified respectively from
697 plasmids pZEP09 (Hautefort et al., 2003), pXG10-SF (Corcoran et al., 2012) and pFCcGi (Figueira et
698 al., 2013). A similar template plasmid, carrying the *frt-aph-frt-tetR-*P_{tetA} module (pNAW55) was
699 constructed and was used to insert the *tetR* repressor and the AHT-inducible promoter P_{tetA} upstream
700 of genes of interest, as reported earlier (Schulte et al., 2019).
701
702 The high copy number plasmid pUC18 was used to clone the different versions of the anti-*bstA* (*aba*)
703 fragment: the *aba* fragments (*aba1-aba14* alleles) were amplified by PCR, digested with EcoRI and
704 BamHI and ligated into the corresponding sites of pUC18. Phagemids based on the phage P22
705 replication module were constructed by EcoRI/KpnI digestion and ligation, as follows: the P_R promoter
706 and the *cro-c1-orf48-O-P* genes of P22 (coordinates 31648-34683) were amplified and circularized by
707 ligation with the *aph* Km^R cassette of pKD4 or with the *aba-aph* / *aba*^{mut1}*-aph* modules, amplified from
708 strain SNW617. The ligations reactions were purified and electroporated into ultra-competent SNW555,
709 a prophage-free and plasmid-free derivative of *S.* Typhimurium D23580. The resulting phagemids
710 pNAW229 (pP22-*aph*), pNAW230 (pP22-*aba-aph*) and pNAW231 (pP22-*aba*^{mut1}*-aph*) were obtained
711 after selection on Km medium.
712
713 Phage DNA was extracted from high titer lysates in LBO: nine volume of the phage lysates were mixed
714 with one volume of 10 X DNase buffer (100 mM Tris-HCl, 25 mM $MgCl_2$, pH 7.5) supplemented with
715 RNase A (40 µg/mL final) and DNase I (400 µg/mL final). After 1 hour incubation at 37°C, DNase I was
716 heat-inactivated at 75°C for 10 min and phage DNA was extracted from 500 µL of the nuclease-treated
717 lysates with the Norgen Phage DNA Isolation after Proteinase K treatment, as specified by the
718 manufacturer.
719
720 **Genome editing techniques**
721 Strain constructions are detailed in Supplementary Table 2. For chromosomal insertions and deletions,
722 *λ red* recombination was carried out with the arabinose-inducible plasmid pKD46 (for *E. coli*) or with the
723 heat inducible plasmid pSIM5-*tet* (for *Salmonella*), both expressing the *λ red* genes. Bacteria were grown
724 to exponential phase in LBO, according to the resistance and induction condition of the respective *λ red*
725 plasmid (Datsenko and Wanner, 2000; Hammarlöf et al., 2018; Koskiniemi et al., 2011) and electro-
726 competent cells were prepared as mentioned above. PCR fragments carrying a resistance cassette
727 were constructed by overlap extension PCR or were directly obtained by PCR from the adequate

728 plasmid. Electro-competent cells (40-50 µL) were transformed with 500-5000 ng of the PCR fragments
729 and the recombinants were selected on selective LB agar plates.
730
731 Mutations or insertions linked to selective markers were transduced into *Salmonella* strains using the
732 P22 HT *105/1 int-201* (P22 HT) transducing phage (Owen et al., 2017; Schmieger, 1972). For *E. coli*,
733 the transducing phage P1 *vir* was used (Ikeda and Tomizawa, 1965; Tiruvadi Krishnan et al., 2015).
734 Transductants were grown on selective LB agar plates supplemented with 10 mM EGTA. After two
735 passages, clearance of the transducing phages was confirmed by diagnostic PCR using primer pairs
736 NW_62/NW_63 for P22 HT or NW_392/NW_393 for P1 *vir* and by a passage on Green Agar medium
737 (Maloy, 1990).To remove the antibiotic cassettes, flanked by FLP recognition target sites (*frt*), the FLP
738 recombinase expressing plasmids pCP20, pCP20-TcR and pCP20-Gm were used, as previously
739 reported (Cherepanov and Wackernagel, 1995; Doublet et al., 2008; Hammarlöf et al., 2018; Kintz et
740 al., 2015). The inducible *tetR-*P_{tetA}*-bstA* modules were constructed by fusing the *frt-aph-frt-tetR-*P_{tetA}
741 module of pNAW55 to the *bstA* gene of D23580 (*bstA*^{BTP1}, *STMMW_03531*), *E. coli* NCTC10963 (*bstA*^{Ec},
742 *E4V89_RS07420*) or *K. pneumoniae* Kp52.145 (*bstA*^{Kp}, *BN49_1470*). Each construct carries the native
743 *bstA* ribosome binding site and Rho-independent terminator. The *tetR-*P_{tetA}*-bstA* modules were inserted
744 by *λ red* recombination into the *STM1553* pseudogene of *S.* Typhimurium LT2 (between coordinates
745 1629109-1629311), corresponding to *STMMW_15481* in D23580 (coordinates 1621832-3). Previously
746 we have shown that the *STM1553* and *STMMW_15481* genes are not expressed at the transcriptional
747 level (Canals et al., 2019).
748
749 In *E. coli* MG1655, the *bstA* modules were inserted into the *glmS-pstS* intergenic region (coordinates
750 3911773-4). To generate Ap and Cm sensitive D23580 strains, the pSLT-BT plasmid-encoded Tn*21*-
751 like element, that carries the resistance genes (Kingsley et al., 2009), was replaced by the Km^R cassette
752 of pDK4 by *λ red* recombination (deletion coordinates 34307 to 57061, GenBank: NC_013437.1). The
753 resulting large single-copy plasmid pSLT-BT ΔTn*21*::*aph* was extracted (Heringa et al., 2007) and
754 electroporated into the strains of interest. After selection on Km medium, the Ap and Cm sensitivity was
755 confirmed and the Km^R cassette was flipped out using pCP20-Gm. For scarless genome editing, the
756 pEMG plasmid-based allelic exchange system was used (Martínez-García and de Lorenzo, 2011). The
757 pEMG derivative suicide plasmids were constructed as specified in Supplementary Table 2 and were
758 replicated in *E. coli* S17-1 *λpir*. Conjugation of the resulting plasmids into S*almonella* and subsequent
759 merodiploid resolution with plasmid pSW-2 were carried out as previously described (Canals et al., 2019;
760 Owen et al., 2017). Some key strains and phages (indicated in Supplementary Table 2) used in this
761 study were whole-genome sequenced (Illumina) at MicrobesNG (Birmingham, UK).
762
763 **Plasmid deletion in *S.* Typhimurium D23580**
764 The pSLT-BT, pBT1, pBT2 and pBT3 plasmids (Kingsley et al., 2009) were cured from strain D23580,
765 using the CRISPR-Cas9-based methodology (Lauritsen et al., 2017). A novel CRISPR-Cas9 Km
766 resistant plasmid (pNAW136) was obtained by ligating the CRISPR-Cas9 module of plasmid pCas9
767 (Jiang et al., 2013) with the unstable origin of replication *ori*RK2, the *trfA* replication gene and the *aph*
768 Km^R gene. Anti-plasmid protospacers (30 bp) were generated by the annealing of 5'-phosphorylated
769 primer pairs that targeted the pSLT-BT, pBT1, pBT2 and pBT3 plasmids, designed according to the
770 Marraffini Lab protocol (Jiang et al., 2013). The protospacers were ligated into *Bsa*I-digested pNAW136
771 with T4 DNA ligase and the resulting plasmids were checked by Sanger sequencing, using primer
772 NW_658.
773
774 The resulting plasmids pNAW168 (anti-pSLT-BT) and pNAW169 (anti-pBT1), pNAW139 (anti-pBT2)
775 and pNAW191 (anti-pBT3) were electroporated into D23580-derived strains and transformants were
776 selected on Km plates. After two passages on Km, the loss of the pSLT-BT, pBT1, pBT2 or pBT3
777 plasmids was confirmed by diagnostic PCR. The absence of the unstable pNAW136-derived plasmids
778 was confirmed by the Km sensitive phenotype of colonies after two passages on non-selective medium.

779 **Phage stock preparation and plaque assays**
780 All phage stocks were prepared in LB or LBO. For *Salmonella* phages, the prophage-free strain *S.*
781 Typhimurium D23580 ΔΦ (JH3949) was used as host (Owen et al., 2017). Exponential phase cultures
782 of D23580 ΔΦ were infected with ~10^5 Plaque Forming Units (PFU) and infected cultures were incubated
783 for at least 3 hours at 37°C (with aeration). Phages lysates were spun down (4,000 X *g*, 15 min) and

784 supernatants were filter-sterilized (0.22 µm, StarLab syringe filters). The resulting phage lysates were
785 stored at 4°C in the presence 1% chloroform to prevent bacterial contamination.
786
787 Coliphage lysates were prepared similarly with *E. coli* MG1655 as host. When required, maltose (0.2%),
788 $CaCl_2$ (10 mM) and $MgSO_4$ (10 mM) were added during the infection (λ, P1 *vir* and Φ80*p*SU3$^+$). For
789 Φ80-derived phages, the infection temperature was reduced to 30°C (Rotman et al., 2010).
790
791 Phage lysates were serial-diluted (decimal dilutions) with LB and virion enumeration was performed by
792 double-layer overlay plaque assay (Kropinski et al., 2009), as follows. Bacterial lawns were prepared
793 with stationary phase cultures of the reporter strains, diluted 40 times with warm Top Agar (0.5 % agar
794 in LB, 50°C). The seeded Top Agar was poured on LB 1.5% agar bottom layer: 4 mL for 8.6 cm diameter
795 petri dishes or 8 mL for 12 x 12 cm square plates.
796
797 When inducible P_{tetA} or P_{BAD} constructs were present in the reporter bacteria, 500 ng/mL of AHT or 0.2
798 % arabinose were added in the Top Agar. When required, antibiotics were added in the Top Agar layer.
799 The bacterial lawns were incubated for 30 min at room temperature with the appropriate inducer, to
800 allow solidification and the expression of the inducible genes. Finally, phages suspensions (5-20 µL)
801 were applied on the Top Agar surface and pictures of the resulting plaques were taken with an
802 ImageQuant Las 4000 imager (GE Healthcare) after 16-20 hours incubation at 30 or 37°C.
803
804 **Construction of P22 virulent phages**
805 For the generation of obligately virulent P22 phages, a 633 bp in-frame deletion (coordinates 31028-
806 31660) was introduced in the *c2* repressor gene by *λ red* recombination in a P22 lysogen as follows.
807 Two fragments of ~500 bp, flanking *c2*, were amplified with primers pairs NW_818 / NW_819 and
808 NW_820 / NW_821. The two amplicons were fused by overlap extension PCR and 1000-3000 ng of the
809 resulting Δ*c2* fragment were electroporated into P22 lysogens (in the prophage-free D23580 ΔΦ
810 background) carrying the *λ red* recombination plasmid pSIM5-*tet*, as described above. The
811 transformation reactions were re-suspended in 5 mL LB and incubated for 2 hours at 37°C with aeration.
812 The culture supernatants were filter sterilized and serial-diluted to 10^{-2}. Ten microliters of each dilution
813 were mixed with 100 µL of a D23580 ΔΦ stationary phase culture and with 4 mL of warm Top Agar. The
814 mixtures were poured on LB agar plates and the plates were incubated for ~16 hours at 37°C. P22 Δ*c2*
815 recombinants were identified by the clear morphology of their plaques, compared to the turbid plaques
816 of WT P22. The Δ*c2* deletion was confirmed by PCR and Sanger sequencing with primers NW_406 and
817 NW_805.
818
819 **Use of the Δ*tsp-gtrAC* genetic background**
820 Where possible, experiments were carried out with native BstA expression (from its natural locus within
821 the BTP1 prophage), to best recapitulate the natural biological activity of the protein. However, as the
822 *gtr* locus of phage BTP1 blocks attachment of many phages including P22 and BTP1, to achieve efficient
823 phage infections we consistently used a strain background where the *gtr* locus has been inactivated
824 (Δ*tsp-gtrAC*). The BTP1 prophage spontaneously induces to a titer of ~10^9 PFU/mL in liquid culture
825 (Owen et al., 2017), and in the absence of *gtr* activity in surrounding cells, free BTP1 phages mediate
826 cleavage of the O-antigen *via* the putative enzymatic activity of the tailspike protein (Kintz et al., 2015).
827 Consequently, to avoid an unnatural, short LPS phenotype as a result of *gtr* inactivation in a BTP1
828 lysogen, we additionally inactivated the upstream gene encoding for the BTP1 tailspike (*tsp*) (D23580
829 Δ*tsp-gtrAC*, JH4287). Full details of the construction of this strain can be found in the Supplementary
830 Resource list.
831
832 **Phage replication assay**
833 Stationary phase cultures of the reporter bacteria were diluted to OD_{600} 0.4 with LB. Aliquots (0.2 mL)
834 were prepared in 1.5 mL tubes and phage stock suspensions were added to a final phage titer of 100-
835 1000 PFU/mL. The infections were carried out at 37°C (30°C for Φ80*p*SU3$^+$) with shaking for 2-4 hours
836 and were stopped by the addition of 20 µL of chloroform. After a 10 sec vortex, the lysates were
837 centrifuged (20,000 X *g*, 5 min) and serial diluted. When M9 Glu$^+$ was used, *Salmonella* strains were
838 grown to OD_{600} ~ 0.5 in this medium prior to phage infection.
839

840 Phage titer was determined by plaque assay: 10 µL of the dilutions were applied to bacterial lawns of
841 the appropriate reporter strain in technical triplicates. Plaques were enumerated after 16-20 hours of
842 incubation and phage titers (PFU/mL) were calculated for each lysate. To measure the phage input at
843 time 0 (T^0), the same volume of stock phage suspension was added to 0.2 mL of bacteria-free LB and
844 the titer was determined as described above. The fold-replication for each phage was calculated as the
845 phage titer of the lysate post infection divided by the input phage titer at T^0. When the phage titer in the
846 lysate was lower than the phage input, the replication was considered to be null ("<1-fold). When AHT
847 inducible *tetR-P*$_{tetA}$*-bstA* strains were used, AHT (500 ng/mL) or methanol (mock) were added to the
848 diluted bacterial suspension and phages were added after 15 min of incubation at 37°C with aeration.
849
850 For replication assays of the coliphages λ, P1 *vir* and Φ80*p*SU3$^+$, *E. coli* strains were grown to
851 exponential phase (OD_{600} 0.4) in LB and phages were added as mentioned above. To stimulate infection
852 by these phages, maltose (0.2%), $CaCl_2$ (10 mM) and $MgSO_4$ (10 mM) were added during the infection
853 and in the lawns of the reporter *E. coli* MG1655. All the phage replication experiments presented were
854 carried out at least twice with biological triplicates.
855
856 **Induction of P22 and BTP1 prophages**
857 D23580 ΔΦ-derived lysogens that carried the different versions of P22 and BTP1 were constructed as
858 detailed in the Supplementary Table 2. For complementation with the pUC18-derived plasmids (Ap^R),
859 Ap sensitive lysogens were constructed by the inactivation of the Tn*21*-like element, as described
860 above. The resulting lysogens were grown to stationary phase in LB and the pre-cultures were diluted
861 1000 times in fresh LB and grown to OD_{600} 0.4-0.5, prior addition of Mitomycin C (MitC, 2 µg/mL). The
862 induced cultures were incubated for 3-5 hours at 37°C with aeration and cultures were filter sterilized
863 and serial diluted. The phage titer was measured by plaque assay on the appropriate host strain lawn
864 with technical replicates, as described above. Phage titers were also measured before MitC induction
865 and the titer of the non-induced culture was subtracted from the induced titer to obtain the final phage
866 titer. All the prophage induction experiments were carried out at least twice with biological triplicates.
867
868 **Survival assays**
869 For the survival assays, D23580 Δ*tsp-gtrAC* (JH4287), D23580 Δ*tsp-gtrAC bstA*^{STOP} (SNW431) or
870 D23580 ΔΦ [P22] (SSO-128) were grown in M9 Glu$^+$ to OD_{600} ~0.5 and two 0.5 mL subcultures were
871 prepared for each culture. The use of D23580 ΔΦ [P22] in these experiments controlled for the effect of
872 lysis from without due to use of high multiplicity of infection (MOI). The strain is a lysogen for WT P22
873 phage, and therefore is highly resistant to infection by P22-derived phages. P22 Δ*c2* was added at an
874 MOI of 5. The same volume of LB was added to the two remaining subcultures (non-infected controls).
875 Samples were incubated for 15 min at 37°C to allow phage attachment. To stop phage development,
876 the cultures were chilled on ice and bacteria were washed with 0.5 mL of cold PBS. All the samples
877 were serial-diluted in PBS to 10^{-6} and kept on ice. For the measure of survival post-infection, 10 µL of
878 diluted infected or non-infected cultures were applied in technical triplicates on LB agar supplemented
879 with 10 mM EGTA (EGTA was used to minimize secondary infection by free phages). Colony forming
880 Units (CFU) were enumerated and the survival rate, was calculated as the ratio of CFUs in infected
881 cultures divided by the CFUs obtained from non-infected cultures (in %). All the survival experiments
882 were carried out at least twice with biological triplicates.
883
884 **Phage DNA detection by Southern Blotting**
885 D23580 ΔΦ *tetR-P*$_{tetA}$*-bstA* (SNW576) was grown in 50 mL LB to OD_{600} ~0.35. The culture was split in
886 two 20 mL sub-cultures and methanol (mock) or AHT (inducer) were added to each subculture. Bacteria
887 were incubated to induce BstA for 20 min at 37°C and the phage of interest was added at an MOI of 5.
888 Infections were carried out at 37°C with aeration and total DNA was extracted (Quick-DNA™ Universal
889 Kit Zymo) from 1.5 mL of culture at 0, 10, 20, 30, 35, 40 and 50 minutes post Infection. Total DNA (100
890 ng, according to QuBit quantification) was size-separated (2 hours at 100 V in TAE 1X) on a 0.8 %
891 agarose-TAE gel containing Midori Green DNA staining (4 µL for 100 mL gel). One hundred nanograms
892 of none-infected D23580 ΔΦ *tetR-P*$_{tetA}$*-bstA* genomic DNA were used as a negative control. DNA was
893 fragmented by exposing the agarose gel to UV light for 5 min on a UV-transilluminator. DNA was
894 denatured by soaking the gel in the Denaturation Solution (0.5 M NaOH, 1.5 M NaCl) for 30 min and
895 then in the Neutralization Solution (1.5 M NaCl, 1 M Tris-HCl, pH 7.6) for 30 min. DNA was transferred
896 on a positively-charged Nylon membrane using the capillary blotting method. Phage DNA was detected

897 with DIG labelled dsDNA probes generated by PCR amplification with MyTaq DNA polymerase (Bioline),
898 buffer, phage DNA and primers (0.4 µM each), in the presence of 0.2 mM dATP, 0.2 mM dCTP, 0.2 mM
899 dGTP, 0.13 mM dTTP and 0.07 mM DIG-11-dUTP. For the 9NA probe a 588 bp PCR fragment was
900 generated with primer pair NW_602 / NW_603 and for the P22/BTP1 probe a 725 bp PCR fragment
901 was generated with primer pair SO-22 / SO-23. The DNA probes were heat-denatured at 95°C for 15
902 min and the DNA-DNA hybridizations were carried out at 45°C for 16 hours in DIG-Easy Hyb buffer. The
903 washing and immunodetection procedures were carried out, as specified in the DIG Application Manual
904 for Filter Hybridization (Roche) and the chemilumiscence signal was detected using an ImageQuant
905 LAS 4000 imager (GE Healthcare). Prior to DNA transfer onto the membrane, the Midori green-stained
906 DNA was visualized under UV and the resulting image was used as a loading control.

907 **Phagemid efficiency of transformation**
908 To avoid a reduction in transformation caused by interference interspecies DNA modification/restriction
909 incompatibilities between *E. coli* and *Salmonella*, all the P22-derived phagemids were replicated and
910 extracted from *S.* Typhimurium SNW555.
911
912 *Salmonella* strains carrying the *tetR-P*$_{tetA}$*-bstA* module were grown in 50 mL LBO culture. When OD_{600}
913 ~0.4 was reached, each culture was split into two 25 mL sub-cultures and methanol (mock) or AHT
914 (inducer) were added to each subculture. Bacteria were incubated for BstA induction during 15 min at
915 37°C. The cultures were incubated on ice for 5 min and bacteria were washed twice with cold water (25
916 mL) and were concentrated in 0.1 mL of ice-cold sterile 10% glycerol. The OD_{600} of each electro-
917 competent cell sample was measured by diluting 10 µL of competent cells with 990 µL of 10% glycerol.
918 Cell concentration was adjusted with 10% glycerol for each sample, according to the sample with the
919 lowest OD_{600}. The competent cells (20 µL) were mixed with 10 ng (estimated by Qubit) of the P22
920 phagemids, pP22 (pNAW229), pP22-*aba* (pNAW230) or pP22-*aba*^{mut1} (pNAW231) and the mixture was
921 incubated on ice until electroporation (2.5 KV). Transformation reactions were re-suspended in 1 mL LB
922 or 1 mL LB + AHT (for the *bstA*-induced bacteria) and were incubated for 60 min at 37°C, for recovery.
923 The transformations were diluted (decimal dilution to 10^{-5}) in LB or LB+AHT and 100 µL of each dilution
924 (including the non-diluted sample) were spread on LB agar Km or LB agar Km+AHT plates. After
925 incubation at 37°C, the number of Km^R transformants was enumerated for each transformation and
926 efficiency of transformation was defined as the number of transformants obtained per ng of phagemid.
927 This experiment was performed with biological triplicates and was repeated twice with LT2 *tetR-P*$_{tetA}$-
928 *bstA* (SNW389) and once with D23580 ΔΦ *tetR-P*$_{tetA}$*-bstA* (SNW576), giving similar results.
929
930 **Microscopy- general**
931 For all imaging experiments, bacteria were sub-cultured in liquid M9 Glu^+ media. All images were
932 collected with a wide field Nikon Eclipse Ti-E inverted microscope equipped with an Okolab Cage
933 Incubator warmed to 37°C with Cargille Type 37 immersion oil. A Nikon CFI Plan Apo DM Lambda 100X
934 1.45 NA Oil objective and a Nikon CFI Plan Apo DM Lambda 20X .75 NA objective were used with
935 Perfect Focus System for maintenance of focus over time. Superfolder GFP, mCherry and SYTOX
936 Orange Nucleic Acid Stain (ThermoFisher) were excited with a Lumencor Spectra X light engine with
937 Chroma FITC (470/24) and mCherry (575/25) filter sets, respectively and collected with a Spectra Sedat
938 Quad filter cube ET435/26M-25 ET515/30M-25 ET595/40M-25 ET705/72M-25 and a Spectra
939 CFP/YFP/mCherry filter cube ET475/20M-25 ET540/21M-25 ET632/60M-25. Images were acquired
940 with an Andor Zyla 4.2 sCMOS controlled with NIS Elements software. For time-lapse experiments,
941 images were collected every 3 minutes (unless specified otherwise) *via* ND acquisition using an
942 exposure time of 100 ms and 50% or 100% illumination power for fluorescence. Multiple stage positions
943 (fields) were collected using the default engine Ti Z. Fields best representing the overall experimental
944 trend with the least technical artefacts were chosen for publication. Gamma, brightness, and contrast
945 were adjusted (identically for compared image sets) using FIJI(Schindelin et al., 2012). The FIJI plug-
946 ins Stack Contrast (Capek et al., 2006) and StackReg (Thevenaz et al., 1998) were used for brightness
947 matching and registering image stacks.
948
949 **Microscopy- agarose pads**
950 Agarose pads were prepared with 2% agarose and M9 Glu^+ media, and mounted on MatTek dishes
951 (No. 1.5 coverslip, 50 mm, 30 mm glass diameter, uncoated). Cells (D23580Δ*tsp-gtrAC* (JH4287) or
952 D23580Δ*tsp-gtrAC bstA*^{STOP} (SNW431) were grown to log phase (OD_{600} ~ 0.4) in M9 Glu^+ at 37°C with

953 shaking (220 RPM), and where required, diluted in fresh M9 Glu^+ to achieve the desired cell density on
954 the agarose pad. For experiments where all cells were infected (Figure 4A), phage P22 Δ*c2* was added
955 at an MOI of 5. Phage adsorption and initial infection was facilitated by incubation at 37°C with shaking
956 for 10 minutes. Subsequently, infected cells were pelleted at 5000 x g and resuspended in ice-cold PBS
957 to pause phage development. Two microliters of chilled, infected cells were spotted onto opposite sides
958 of an agarose pad (two strains were imaged on the same pad) and inverted onto the MatTek imaging
959 dish. Experimental MOIs were immediately confirmed by CFU and PFU /mL measurement of the cell
960 and phage preparations. Phase-contrast images using the 100X objective were collected every 3
961 minutes for 3 hours.
962
963 Procedures for experiments involving a subset of infected cells (Figure 4C) were identical, except cells
964 infected with P22 Δ*c2 p-mcherry* were washed an additional 4 times in ice-cold PBS to reduce the
965 concentration of un-adsorbed, free phage. In parallel, uninfected cells were washed once in ice-cold
966 PBS. Infected cells were mixed at a ratio of 1:1000 with uninfected cells of the same genotype before
967 being spotted onto the agarose pad. For these experiments, phase-contrast and fluorescence images
968 (mCherry) using the 20X objective were collected every 3 minutes for 3 hours.
969
970 **Microscopy- microfluidic infection**
971 The CellASIC ONIX2 system from EMD Millipore with B04A plates was used for microfluidic imaging
972 experiments (Figure 5). Phages used in microfluidic infection experiments shown in 5B (P22 HT or 9NA)
973 were stained with SYTOX Orange Nucleic Acid Stain according to the protocol previously described
974 (Valen et al., 2012). Stained phages washed 4 times in 15 mL M9 Glu^+ media using Amicon Utra-15
975 centrifugal filter units. After staining, the titer and viability of phages were immediately assessed by
976 plaque assay, and once stained, phages were used for no longer than 2 weeks. For use in the
977 microfluidic experiments, SYTOX Orange strained phages were normalised to a titer of approximately
978 10^{10} PFU/mL. Cells (D23580 *bstA-$_{sf}$gfp,* SNW403) were grown to early exponential phase (OD_{600} ~ 0.1)
979 in M9 Glu^+ at 37°C with shaking (220 RPM) before being loaded into CellASIC B04A plates using the
980 pressure-driven method according to the manufacturer protocol for bacterial cells. The slanted chamber
981 of the plate immobilises the cells, but allows media to flow continuously. Firstly, cells were equilibrated
982 with constant M9 Glu^+ media flow for approximately 30 minutes. Secondly, stained phages suspended
983 in M9 Glu^+ media were flowed over the cells until the majority of cells were infected (typically 10-30
984 minutes). In the case of P22 HT phage (which exhibits inefficient adsorption to D23580 *bstA-$_{sf}$gfp* due
985 to the *gtr* locus of prophage BTP), phages were continuously flowed. Finally, M9 Glu^+ media was flowed
986 over the cells for the duration of the experiment. Microfluidic experiments typically lasted 5 hours, after
987 which time uninfected cells outgrew the chamber. Phase-contrast and fluorescence images were
988 collected every 1.5 minutes for the experiments in Figure 5B.
989
990 For the microfluidic imaging experiments shown in Figure 5C, strain SVO251 (S. Typhimurium D23580
991 ΔΦ *STM1553*::(*P_{tetA}-bstA-$_{sf}$gfp-frt*) ΔpSLT-BT ΔpBT1 pAW61 (*P_{BAD}-parB-mcherry*) was used. This strain
992 contains the *bstA-$_{sf}$gfp* fusion contrast under the control of the *P_{tetA}* promoter. However, this strain lacks
993 the *tetR* gene, and therefore expression of *bstA-$_{sf}$gfp* is constitutive (not inducible). Additionally, this
994 strain is cured of two natural plasmids that contain native partitioning systems (pSLT-BT and pBT1),
995 and there for might interfere with the correct function of the ParB-*parS* system used for phage DNA
996 localization. The ParB-mCherry fusion protein is expressed from the pAW61 plasmid (Ap^R) under the
997 control of the P_{BAD} promoter (induced by L-arabinose). Strain SVO251 was grown in M9 Glu^+
998 supplemented with 100 µg/mL ampicillin to maintain the pAW61 plasmid and 0.2% L-arabinose to induce
999 expression of ParB-mCherry. The same supplemented media was used in the microfluidic chamber.
000 Cells were grown to ~OD600 0.1 before loading into the CellASIC B04A plate as described above. After
001 15 minutes growth, phage P22 *Δpid::*(*parS-aph*) [which contains one parS site along with a kanamycin
002 resistance locus, *aph*, in place of the non-essential *pid* locus (Cenens et al., 2013)] diluted to a
003 concentration of 10^8 PFU/mL (in M9 Glu^+ amp100 0.2% L-ara) was flowed into the chamber. Phase
004 contrast and red and green fluorescence images were collected every 2 minutes for 4 hours.
005
006 **BstA protein homolog analysis**
007 BstA protein homologs were identified using tblastn (database: non-redundant nucleotide collection)
008 and the HMMER webserver (Potter et al., 2018) (database: Reference Proteomes). The dataset of BstA
009 protein homologs was manually curated to reflect the diversity of taxonomic background harbouring

homologs. To analyse the genetic context of BstA homologs, the sequence region 20 Kb either side of the homolog (40 kb total) was extracted (BstA 40 kb neighbourhoods). To produce homogenous and comparable annotations, each region was re-annotated using Prokka 1.13 (Seemann, 2014). Additionally, the resulting annotated amino acid sequences were queried against our custom BstA profile-hmm and the Pfam 31.0 database (El-Gebali et al., 2019) with hmmerscan (Eddy, 1998), and the highest scoring significant hit per ORF was considered for the results shown in Figure 2. All the code is available in https://github.com/baymLab/2020_Owen-BstA.

Pairwise identity of homologs in Figure 2B to $BstA^{BTP1}$ was computed using the EMBOSS Needle webserver (Needleman and Wunsch, 1970). BstA homologs were designated "putatively-prophage associated" if annotated genes in the 40 kb neighbourhood contained any instance or the word "phage" or "terminase". For categorisation in Figure 2C, homologs were classed as having "high confidence association" if instances of gene annotations including the aforementioned key words occurred both before, and after, the BstA gene within the 40 Kb neighbourhood (i.e., to account for the possibility that a prophage-independent homolog could co-occur next to a prophage region by chance). Homologs classed as having "low confidence association" had at least one instance of genes whose annotations included "phage" or "terminase" either in the upstream or downstream 20Kb, but not both. Plasmid status was determined from information in the sequence records. The HHpred webserver was used to annotate the putative KilA-N domain (Zimmermann et al., 2018). All homolog neighbourhoods, homolog alignments and sequences is available to download https://github.com/baymLab/2020_Owen-BstA.

QUANTIFICATION AND STATISTICAL ANALYSES

The phage replication, survival rate, efficiencies of transformation and of lysogeny were calculated as mentioned above. The numerical data were plotted and analyzed using GraphPad Prism 8.4.1. Unless stated otherwise in the figure legends, data are presented as the mean of biological triplicates ± standard deviation. The unpaired *t*-test was used to compare the groups and statistical significance is indicated on the figures. P values are reported using the following criteria: < 0.0001 = ****, 0.0001 to 0.001 = ***, 0.001 to 0.01 = **, 0.01 to 0.05 = *, ≥ 0.05 = ns.

038 **KEY RESOURCES TABLE**

REAGENT or RESOURCE	SOURCE	IDENTIFIER
Antibodies		
Anti-Digoxigenin-AP, Fab fragments (Roche)	MilliporeSigma	Cat#00000001109327 4910
Bacterial and Virus Strains		
All the bacterial strains and bacteriophages are listed and described in Supplementary Table 2		
Chemicals, Peptides, and Recombinant Proteins		
L-(+)-arabinose	Melford	Cat#A51000-100.0
Betaine	MilliporeSigma	Cat#B2629
Bacto Agar (BD)	Appleton Woods	Cat#MN663
Bacto Casamino Acids Technical (BD)	Appleton Woods	Cat#223110
EGTA	MilliporeSigma	Cat#E3889
M9 Salts 5X	MilliporeSigma	Cat#M6030
Maltose	MilliporeSigma	Cat#M5885
m-toluic acid	MilliporeSigma	Cat#T36609
Tryptone (BD)	Appleton Woods	Cat#MN649
Yeast Extract (BD)	Appleton Woods	Cat#DM832
Ampicillin Sodium	Melford	Cat#A40040-25.0
Anhydrotetracycline hydrochloride (AHT)	MilliporeSigma	Cat#37919
Chloramphenicol	MilliporeSigma	Cat#C0378
Gentamicin sulfate	Melford	Cat#G38000-25.0
Kanamycin monosulfate	Melford	Cat#K22000-25.0
Mitomycin C	MilliporeSigma	Cat#M0503
Tetracycline hydrochloride	MilliporeSigma	Cat#T7660
EcoRI	ThermoFisher Scientific	Cat#ER0271
BamHI	ThermoFisher Scientific	Cat#ER0051
DpnI	New England Biolabs	Cat#R0176S
KpnI-HF	New England Biolabs	Cat#R3142S
BsaI-HF	New England Biolabs	Cat#R3535S
SmaI	ThermoFisher Scientific	Cat#ER0661
SalI	ThermoFisher Scientific	Cat#ER0641
XbaI	New England Biolabs	Cat#R0145S
T4 Polynucleotide Kinase	ThermoFisher Scientific	Cat#EK0031
T4 DNA ligase	ThermoFisher Scientific	Cat#EL0014
CutSmart buffer	New England Biolabs	Cat#B7204S
Tango Buffer 10X	ThermoFisher Scientific	Cat#BY5
T4 DNA ligase Reaction Buffer	New England Biolabs	Cat#B0202S
Phusion High Fidelity DNA polymerase	New England Biolabs	Cat#M0530S
MyTaq Red PCR mix 2X	Bioline	Cat#BIO-25043
Taq DNA polymerase	Bioline	Cat#BIO-21105
DNase I	MilliporeSigma	Cat#DN25
RNase A	MilliporeSigma	Cat#R6513
Proteinase K	Bioline	Cat#BIO-37037
dNTP mix	Bioline	Cat#BIO-39025
dATP	Bioline	Cat#BIO-39036
dGTP	Bioline	Cat#BIO-39037
dCTP	Bioline	Cat#BIO-39038
dTTP	Bioline	Cat#BIO-39039
DIG-11-dUTP, alkali-stable (Roche)	MilliporeSigma	Cat#11093088910
Midori Green DNA/RNA staining	Nippon Genetics	Cat#MG06
Electroporation cuvettes	Geneflow	Cat#E6-0060
Nylon membrane, positively charged (Roche)	MilliporeSigma	Cat#11417240001

Blocking Reagent (Roche)	MilliporeSigma	Cat#11096176001
DIG Easy Hyb™ Granules (Roche)	MilliporeSigma	Cat#11796895001
Critical Commercial Assays		
ISOLATE II Plasmid Mini Kit	Bioline	Cat#BIO-52057
ISOLATE II PCR and Gel Kit	Bioline	Cat#BIO-52060
Norgen Phage DNA Isolation Kit (46850)	GeneFlow	Cat#P4-0134
Quick-DNA™ Universal Kit	Zymo	Cat#D4069
Invitrogen Qubit dsDNA HS Assay Kit	ThermoFisher Scientific	Cat#Q32851
SYTOX Orange Nucleic Acid Stain – 5 mM in DMSO	ThermoFisher Scientific	Cat#S11368
Amicon Ultra-15 centrifugal filter units	MilliporeSigma	Cat#UFC910024
Oligonucleotides		
All the DNA oligonucleotides are listed in Supplementary Table 2		
Recombinant DNA		
All the plasmids are listed and described in Supplementary Table 2		
Software and Algorithms		
GraphPad Prism 8.4.1		
HMMER webserver	https://www.ebi.ac.uk/Tools/hmmer/	
Prokka 1.13		
HHPred webserver	https://toolkit.tuebingen.mpg.de/tools/hhpred	
EMBOSS Needle webserver	https://www.ebi.ac.uk/Tools/psa/emboss_needle/	

Acknowledgements

We are grateful to present and former members of the Hinton and Baym laboratories, except Lizeth Lacharme Lora, for helpful discussions, and Paul Loughnane for his expert technical assistance. We thank the Bollback Lab (Liverpool) for the gift of pCas9 and P1*vir*, Allison Lab (Liverpool) for MG1655 and T4, Casadesus Lab (Seville) for 9NA and Det7, Ansaldi Lab (Marseille) for T5, Penadés Lab (Glasgow) for ES18, and Klumpp Lab (Zurich) for FelixO1. We also acknowledge all the other kind labs who responded to our call for *Salmonella* and *E. coli* phages. We thank Benoît Doublet for the gift of pCP20-Gm. We thank the David Van Valen lab, Francois St-Pierre and Paul Wiggins lab for λFS135 and pAW62.

Research in this publication was supported by a Wellcome Trust Senior Investigator award (to JCDH, grant number 106914/Z/15/Z), NIGMS of the National Institutes of Health (to MB, award number R35GM133700) and the David and Lucile Packard Foundation (SVO, NQO, and MB).

References

Abedon, S.T. (2012). Bacterial ‘immunity’ against bacteriophages. Bacteriophage *2*, 50–54.

Barth, Z.K., Silvas, T.V., Angermeyer, A., and Seed, K.D. (2020). Genome replication dynamics of a bacteriophage and its satellite reveal strategies for parasitism and viral restriction. Nucleic Acids Res *48*, 249–263.

Bialek-Davenet, S., Criscuolo, A., Ailloud, F., Passet, V., Jones, L., Delannoy-Vieillard, A.S., Garin, B., Hello, S. Le, Arlet, G., Nicolas-Chanoine, M.H., et al. (2014). Genomic definition of hypervirulent and multidrug-resistant *klebsiella pneumoniae* clonal groups. Emerging Infectious Diseases.

Bingham, R., Ekunwe, S.I., Falk, S., Snyder, L., and Kleanthous, C. (2000). The major head protein of bacteriophage T4 binds specifically to elongation factor Tu. J. Biol. Chem. *275*, 23219–23226.

Bondy-Denomy, J., and Davidson, A.R. (2014). When a virus is not a parasite: the beneficial effects of prophages on bacterial fitness. J Microbiol. *52*, 235–242.

Brüssow, H., Canchaya, C., and Hardt, W.-D. (2004). Phages and the Evolution of Bacterial Pathogens: from Genomic Rearrangements to Lysogenic Conversion. Microbiol Mol Biol Rev *68*, 560–602.

Canals, R., Hammarlöf, D.L., Kröger, C., Owen, S.V., Fong, W.Y., Lacharme-Lora, L., Zhu, X., Wenner, N., Carden, S.E., Honeycutt, J., et al. (2019). Adding function to the genome of African Salmonella Typhimurium ST313 strain D23580. PLOS Biology *17*, e3000059.

Capek, M., Janácek, J., and Kubínová, L. (2006). Methods for compensation of the light attenuation with depth of images captured by a confocal microscope. Microsc. Res. Tech. *69*, 624–635.

Cenens, W., Mebrhatu, M.T., Makumi, A., Ceyssens, P.-J., Lavigne, R., Van Houdt, R., Taddei, F., and Aertsen, A. (2013). Expression of a novel P22 ORFan gene reveals the phage carrier state in Salmonella typhimurium. PLoS Genet. *9*, e1003269.

Cherepanov, P.P., and Wackernagel, W. (1995). Gene disruption in *Escherichia coli*: Tc^R and Km^R cassettes with the option of Flp-catalyzed excision of the antibiotic-resistance determinant. Gene.

Chopin, M.-C., Chopin, A., and Bidnenko, E. (2005). Phage abortive infection in lactococci: variations on a theme. Current Opinion in Microbiology *8*, 473–479.

Cohen, D., Melamed, S., Millman, A., Shulman, G., Oppenheimer-Shaanan, Y., Kacen, A., Doron, S., Amitai, G., and Sorek, R. (2019). Cyclic GMP–AMP signalling protects bacteria against viral infection. Nature *574*, 691–695.

Corcoran, C.P., Podkaminski, D., Papenfort, K., Urban, J.H., Hinton, J.C.D., and Vogel, J. (2012). Superfolder GFP reporters validate diverse new mRNA targets of the classic porin regulator, MicF RNA. Molecular Microbiology.

Datsenko, K.A., and Wanner, B.L. (2000). One-step inactivation of chromosomal genes in *Escherichia coli* K-12 using PCR products. Proceedings of the National Academy of Sciences of the United States of America.

Dedrick, R.M., Jacobs-Sera, D., Guerrero Bustamante, C.A., Garlena, R.A., Mavrich, T.N., Pope, W.H., Reyes, J.C.C., Russell, D.A., Adair, T., Alvey, R., et al. (2017). Prophage-mediated defense against viral attack and viral counter-defense. Nat Microbiol *2*, 16251.

Degnan, P.H., Michalowski, C.B., Babić, A.C., Cordes, M.H.J., and Little, J.W. (2007). Conservation and diversity in the immunity regions of wild phages with the immunity specificity of phage lambda. Mol. Microbiol. *64*, 232–244.

097 Dinsmore, P.K., and Klaenhammer, T.R. (1997). Molecular characterization of a genomic region in a
098 Lactococcus bacteriophage that is involved in its sensitivity to the phage defense mechanism AbiA.
099 Journal of Bacteriology *179*, 2949–2957.

100 Doublet, B., Douard, G., Targant, H., Meunier, D., Madec, J.Y., and Cloeckaert, A. (2008). Antibiotic
101 marker modifications of λ Red and FLP helper plasmids, pKD46 and pCP20, for inactivation of
102 chromosomal genes using PCR products in multidrug-resistant strains. Journal of Microbiological
103 Methods.

104 Durmaz, E., and Klaenhammer, T.R. (2007). Abortive Phage Resistance Mechanism AbiZ Speeds the
105 Lysis Clock To Cause Premature Lysis of Phage-Infected Lactococcus lactis. Journal of Bacteriology
106 *189*, 1417–1425.

107 Eddy, S.R. (1998). Profile hidden Markov models. Bioinformatics *14*, 755–763.

108 Edwards, R.A., Allen Helm, R., and Maloy, S.R. (1999). Increasing DNA transfer efficiency by
109 temporary inactivation of host restriction. BioTechniques.

110 El-Gebali, S., Mistry, J., Bateman, A., Eddy, S.R., Luciani, A., Potter, S.C., Qureshi, M., Richardson,
111 L.J., Salazar, G.A., Smart, A., et al. (2019). The Pfam protein families database in 2019. Nucleic Acids
112 Res. *47*, D427–D432.

113 Van Den Ent, F., and Löwe, J. (2006). RF cloning: A restriction-free method for inserting target genes
114 into plasmids. Journal of Biochemical and Biophysical Methods.

115 Figueira, R., Watson, K.G., Holden, D.W., and Helaine, S. (2013). Identification of *Salmonella*
116 pathogenicity island-2 type III secretion system effectors involved in intramacrophage replication of *S.*
117 *enterica* serovar Typhimurium: Implications for rational vaccine design. MBio.

118 Fineran, P.C., Blower, T.R., Foulds, I.J., Humphreys, D.P., Lilley, K.S., and Salmond, G.P.C. (2009).
119 The phage abortive infection system, ToxIN, functions as a protein-RNA toxin-antitoxin pair. Proc.
120 Natl. Acad. Sci. U.S.A. *106*, 894–899.

121 Fortier, L.-C., and Sekulovic, O. (2013). Importance of prophages to evolution and virulence of
122 bacterial pathogens. Virulence *4*, 354–365.

123 Fujisawa, H., and Morita, M. (1997). Phage DNA packaging. Genes to Cells *2*, 537–545.

124 Gerlach, R.G., Hölzer, S.U., Jäckel, D., and Hensel, M. (2007). Rapid engineering of bacterial reporter
125 gene fusions by using red recombination. Applied and Environmental Microbiology.

126 Green, R., and Rogers, E.J. (2014). Chemical Transformation of *E. coli*. Methods Enzymol. 329–336.

127 Hammarlöf, D.L., Kröger, C., Owen, S. V., Canals, R., Lacharme-Lora, L., Wenner, N., Schager, A.E.,
128 Wells, T.J., Henderson, I.R., Wigley, P., et al. (2018). Role of a single noncoding nucleotide in the
129 evolution of an epidemic African clade of *Salmonella*. Proceedings of the National Academy of
130 Sciences of the United States of America.

131 Hampton, H.G., Watson, B.N.J., and Fineran, P.C. (2020). The arms race between bacteria and their
132 phage foes. Nature *577*, 327–336.

133 Hansen, E.B. (1989). Structure and regulation of the lytic replicon of phage P1. Journal of Molecular
134 Biology *207*, 135–149.

135 Hautefort, I., Proença, M.J., and Hinton, J.C.D. (2003). Single-Copy Green Fluorescent Protein Gene
136 Fusions Allow Accurate Measurement of *Salmonella* Gene Expression In Vitro and during Infection of
137 Mammalian Cells. Applied and Environmental Microbiology.

138 Heckman, K.L., and Pease, L.R. (2007). Gene splicing and mutagenesis by PCR-driven overlap
139 extension. Nature Protocols.

140 Heringa, S., Monroe, J., and Herrick, J. (2007). A Simple, Rapid Method for Extracting Large Plasmid
141 DNA from Bacteria. Nature Precedings.

142 Herrero-Fresno, A., Wallrodt, I., Leekitcharoenphon, P., Olsen, J.E., Aarestrup, F.M., and Hendriksen,
143 R.S. (2014). The Role of the st313-td Gene in Virulence of Salmonella Typhimurium ST313. PLoS
144 One *9*.

145 Herrero-Fresno, A., Espinel, I.C., Spiegelhauer, M.R., Guerra, P.R., Andersen, K.W., and Olsen, J.E.
146 (2018). The Homolog of the Gene bstA of the BTP1 Phage from Salmonella enterica Serovar
147 Typhimurium ST313 Is an Antivirulence Gene in Salmonella enterica Serovar Dublin. Infect. Immun.
148 *86*.

149 Howard-Varona, C., Hargreaves, K.R., Abedon, S.T., and Sullivan, M.B. (2017). Lysogeny in nature:
150 mechanisms, impact and ecology of temperate phages. The ISME Journal *11*, 1511–1520.

151 Ikeda, H., and Tomizawa, J. (1965). Transducing fragments in generalized transduction by phage P1.
152 Journal of Molecular Biology.

153 Iyer, L.M., Koonin, E.V., and Aravind, L. (2002). Extensive domain shuffling in transcription regulators
154 of DNA viruses and implications for the origin of fungal APSES transcription factors. Genome Biology
155 *3*, research0012.1.

156 Jiang, W., Bikard, D., Cox, D., Zhang, F., and Marraffini, L.A. (2013). RNA-guided editing of bacterial
157 genomes using CRISPR-Cas systems. Nature Biotechnology.

158 Kingsley, R.A., Msefula, C.L., Thomson, N.R., Kariuki, S., Holt, K.E., Gordon, M.A., Harris, D., Clarke,
159 L., Whitehead, S., Sangal, V., et al. (2009). Epidemic multiple drug resistant *Salmonella* Typhimurium
160 causing invasive disease in sub-Saharan Africa have a distinct genotype. Genome Research.

161 Kintz, E., Davies, M.R., Hammarlöf, D.L., Canals, R., Hinton, J.C.D., and van der Woude, M.W.
162 (2015). A BTP1 prophage gene present in invasive non-typhoidal *Salmonella* determines composition
163 and length of the O-antigen of the lipopolysaccharide. Molecular Microbiology.

164 Koskiniemi, S., Pränting, M., Gullberg, E., Näsvall, J., and Andersson, D.I. (2011). Activation of cryptic
165 aminoglycoside resistance in *Salmonella enterica*. Molecular Microbiology.

166 Kropinski, A.M., Mazzocco, A., Waddell, T.E., Lingohr, E., and Johnson, R.P. (2009). Enumeration of
167 bacteriophages by double agar overlay plaque assay. Methods in Molecular Biology (Clifton, N.J.).

168 Labrie, S.J., Samson, J.E., and Moineau, S. (2010). Bacteriophage resistance mechanisms. Nature
169 Reviews Microbiology *8*, 317–327.

170 Lauritsen, I., Porse, A., Sommer, M.O.A., and Nørholm, M.H.H. (2017). A versatile one-step CRISPR-
171 Cas9 based approach to plasmid-curing. Microbial Cell Factories.

172 Lopatina, A., Tal, N., and Sorek, R. (2020). Abortive Infection: Bacterial Suicide as an Antiviral
173 Immune Strategy. Annual Review of Virology *7*, null.

174 Maloy, S.R. (1990). Experimental techniques in bacterial genetics (Boston, MA).

175 Martínez-García, E., and de Lorenzo, V. (2011). Engineering multiple genomic deletions in Gram-
176 negative bacteria: Analysis of the multi-resistant antibiotic profile of *Pseudomonas putida* KT2440.
177 Environmental Microbiology.

178 Maxwell, K.L. (2017). The Anti-CRISPR Story: A Battle for Survival. Molecular Cell *68*, 8–14.

179 McClelland, M., Sanderson, K.E., Spieth, J., Clifton, S.W., Latreille, P., Courtney, L., Porwollik, S., Ali,
180 J., Dante, M., Du, F., et al. (2001). Complete genome sequence of *Salmonella enterica* serovar
181 Typhimurium LT2. Nature.

182 Medina, E.M., Walsh, E., and Buchler, N.E. (2019). Evolutionary innovation, fungal cell biology, and
183 the lateral gene transfer of a viral KilA-N domain. Current Opinion in Genetics & Development *58–59*,
184 103–110.

185 Meeske, A.J., Nakandakari-Higa, S., and Marraffini, L.A. (2019). Cas13-induced cellular dormancy
186 prevents the rise of CRISPR-resistant bacteriophage. Nature *570*, 241–245.

187 Needleman, S.B., and Wunsch, C.D. (1970). A general method applicable to the search for similarities
188 in the amino acid sequence of two proteins. J. Mol. Biol. *48*, 443–453.

189 Owen, S. V., Wenner, N., Canals, R., Makumi, A., Hammarlöf, D.L., Gordon, M.A., Aertsen, A.,
190 Feasey, N.A., and Hinton, J.C.D. (2017). Characterization of the prophage repertoire of African
191 *Salmonella* Typhimurium ST313 reveals high levels of spontaneous induction of novel phage BTP1.
192 Frontiers in Microbiology.

193 Owen, S.V., Canals, R., Wenner, N., Hammarlöf, D.L., Kröger, C., and Hinton, J.C.D. (2020). A
194 window into lysogeny: revealing temperate phage biology with transcriptomics. Microbial Genomics.

195 Parma, D.H., Snyder, M., Sobolevski, S., Nawroz, M., Brody, E., and Gold, L. (1992). The Rex system
196 of bacteriophage lambda: tolerance and altruistic cell death. Genes Dev. *6*, 497–510.

197 Pedulla, M.L., Ford, M.E., Karthikeyan, T., Houtz, J.M., Hendrix, R.W., Hatfull, G.F., Poteete, A.R.,
198 Gilcrease, E.B., Winn-Stapley, D.A., and Casjens, S.R. (2003). Corrected sequence of the
199 bacteriophage P22 genome. Journal of Bacteriology.

200 Potter, S.C., Luciani, A., Eddy, S.R., Park, Y., Lopez, R., and Finn, R.D. (2018). HMMER web server:
201 2018 update. Nucleic Acids Res *46*, W200–W204.

202 Riley, M., Abe, T., Arnaud, M.B., Berlyn, M.K.B., Blattner, F.R., Chaudhuri, R.R., Glasner, J.D.,
203 Horiuchi, T., Keseler, I.M., Kosuge, T., et al. (2006). *Escherichia coli* K-12: A cooperatively developed
204 annotation snapshot - 2005. Nucleic Acids Research.

205 Rostøl, J.T., and Marraffini, L. (2019). (Ph)ighting Phages: How Bacteria Resist Their Parasites. Cell
206 Host Microbe *25*, 184–194.

207 Rotman, E., Amado, L., and Kuzminov, A. (2010). Unauthorized horizontal spread in the laboratory
208 environment: The tactics of Lula, a temperate lambdoid bacteriophage of *Escherichia coli*. PLoS ONE.

209 Sambrook, J., and Russell, D.W. (2001). Molecular Cloning: A Laboratory Manual, Third Edition. In
210 Molecular Cloning: A Laboratory a Manual, p.

211 Samson, J.E., Magadán, A.H., Sabri, M., and Moineau, S. (2013). Revenge of the phages: defeating
212 bacterial defences. Nature Reviews Microbiology *11*, 675–687.

213 Schindelin, J., Arganda-Carreras, I., Frise, E., Kaynig, V., Longair, M., Pietzsch, T., Preibisch, S.,
214 Rueden, C., Saalfeld, S., Schmid, B., et al. (2012). Fiji: an open-source platform for biological-image
215 analysis. Nature Methods *9*, 676–682.

216 Schmieger, H. (1972). Phage P22-mutants with increased or decreased transduction abilities. MGG
217 Molecular & General Genetics.

218 Schulte, M., Sterzenbach, T., Miskiewicz, K., Elpers, L., Hensel, M., and Hansmeier, N. (2019). A
219 versatile remote control system for functional expression of bacterial virulence genes based on the
220 *tetA* promoter. International Journal of Medical Microbiology.

221 Seemann, T. (2014). Prokka: rapid prokaryotic genome annotation. Bioinformatics *30*, 2068–2069.

222 Shub, D.A. (1994). Bacterial Viruses: Bacterial altruism? Current Biology *4*, 555–556.

223 Simon, R., Priefer, U., and Pühler, A. (1983). A broad host range mobilization system for *in vivo*
224 genetic engineering: Transposon mutagenesis in gram negative bacteria. Bio/Technology.

225 Snyder, L. (1995). Phage-exclusion enzymes: a bonanza of biochemical and cell biology reagents?
226 Molecular Microbiology *15*, 415–420.

227 Spiegelhauer, M.R., García, V., Guerra, P.R., Olsen, J.E., and Herrero-Fresno, A. (2020). Association
228 of the prophage BTP1 and the prophage-encoded gene, bstA, with antivirulence of Salmonella
229 Typhimurium ST313. Pathog Dis *78*.

230 St-Pierre., F. (2009). Determination of cell fate selection during phage lambda Infection. Thesis.
231 Massachusetts Institute of Technology.

232 Thevenaz, P., Ruttimann, U.E., and Unser, M. (1998). A pyramid approach to subpixel registration
233 based on intensity. Trans. Img. Proc. *7*, 27–41.

234 Tiruvadi Krishnan, S., Moolman, M.C., van Laar, T., Meyer, A.S., and Dekker, N.H. (2015). Essential
235 validation methods for *E. coli* strains created by chromosome engineering. Journal of Biological
236 Engineering.

237 Trasanidou, D., Gerós, A.S., Mohanraju, P., Nieuwenweg, A.C., Nobrega, F.L., and Staals, R.H.J.
238 (2019). Keeping crispr in check: diverse mechanisms of phage-encoded anti-crisprs. FEMS Microbiol
239 Lett *366*.

240 Trinh, J.T., Székely, T., Shao, Q., Balázsi, G., and Zeng, L. (2017). Cell fate decisions emerge as
241 phages cooperate or compete inside their host. Nature Communications *8*, 14341.

242 Valen, D.V., Wu, D., Chen, Y.-J., Tuson, H., Wiggins, P., and Phillips, R. (2012). A Single-Molecule
243 Hershey-Chase Experiment. Current Biology : CB *22*, 1339.

244 Watson, B.N.J., Vercoe, R.B., Salmond, G.P.C., Westra, E.R., Staals, R.H.J., and Fineran, P.C.
245 (2019). Type I-F CRISPR-Cas resistance against virulent phages results in abortive infection and
246 provides population-level immunity. Nature Communications *10*, 5526.

247 Weigel, C., and Seitz, H. (2006). Bacteriophage replication modules. FEMS Microbiol Rev *30*, 321–
248 381.

249 Zimmermann, L., Stephens, A., Nam, S.-Z., Rau, D., Kübler, J., Lozajic, M., Gabler, F., Söding, J.,
250 Lupas, A.N., and Alva, V. (2018). A Completely Reimplemented MPI Bioinformatics Toolkit with a New
251 HHpred Server at its Core. Journal of Molecular Biology *430*, 2237–2243.

252 Zinder, N.D., and Lederberg, J. (1952). Genetic exchange in *Salmonella*. Journal of Bacteriology *64*,
253 679–699.

Figure legends & Supplementary Materials

Supplementary Table 1: Details of all BstA homologs used in the analysis presented in Figure 2.

Supplementary Table 2: Details of all oligonucleotide sequences, plasmids, bacterial strains and phages used in this study.

Supplementary Video 1: Cells natively expressing BstA (D23580 Δ*tsp-gtrAC*, JH4287) or possessing a mutated BstA locus (D23580 Δ*tsp-gtrAC bstA*^{STOP}, SNW431) were infected with the obligately virulent P22-derivate phage, P22Δ*c2*, at an MOI of 5 (to increase the likelihood of infecting all cells). Infected cells were imaged every 3 minutes on agarose pads. Regardless of BstA function, almost all cells were observed to lyse (indicated by loss of defined cell shape and phase contrast).

Supplementary Video 2: Cells natively expressing BstA (D23580 Δ*tsp-gtrAC*, JH4287) or possessing a mutated BstA locus (D23580 Δ*tsp-gtrAC bstA*^{STOP}, SNW431) were infected with the obligately virulent P22-derivate phage, P22Δ*c2 p-mcherry*, at an MOI of 5 (to increase the likelihood of infecting all cells). Due to the *mcherry* insertion, red fluorescence corresponds to phage replication. Infected cells were mixed 1:1000 with uninfected cells. Cells mixtures were imaged every 5 minutes on agarose pads for 6 hours. In the BstA+ cells, primary infected cells lysed, but did not stimulate secondary infections of neighbouring cells, and eventually formed a confluent lawn. In BstA- cells, primary lysis events caused secondary infections (neighbouring cells showing red fluorescence and subsequent lysis) causing an epidemic of phage infection reminiscent of plaque formation.

Supplementary Video 3: Cells natively expressing BstA translationally fused to $_{sf}$GFP (D23580 *bstA-*$_{sf}$*gfp,* SNW403) were grown in a microfluidic growth chamber and imaged every 1.5 minutes. Fluorescently labelled phages P22 HT (left) or 9NA (right) were then added to the cells, and can be seen adsorping to cells as red fluorescent puncta. For purposes of comparison, timestamps are synchronised to the point at which phage are first observed. Typically around 20 minutes after initial observation of phage infection, BstA proteins formed discrete and dynamic foci within the. Cells then proceeded to lyse.

Supplementary Video 4: Cells heterologously expressing BstA translationally fused to $_{sf}$GFP, and ParB translationally fused to mCherry (D23580 ΔΦ ΔpSLT_BT ΔpBT1 STMMW_15481::[PtetA-bstABTP1-sfgfp-frt] pAW61, SVO251) were grown in a microfluidic growth chamber and imaged every 2 minutes**.** Phage P22 ∆pid::(parS-aph) were then added to the cells. ParB protein oligomerises onto DNA at *parS* sites, and therefore *parS*-tagged DNA is indicated by ParB-mCherry foci (red). Translocation of infecting phage DNA is indicated by the formation of red foci within the cells, which is rapidly followed by formation of green, BstA foci. The green and red foci appear to physically overlap. Infected cells proceed to lyse. The same timeseries is presented as separate channels (phase contrast, GFP, mCherry), and a composite merge.

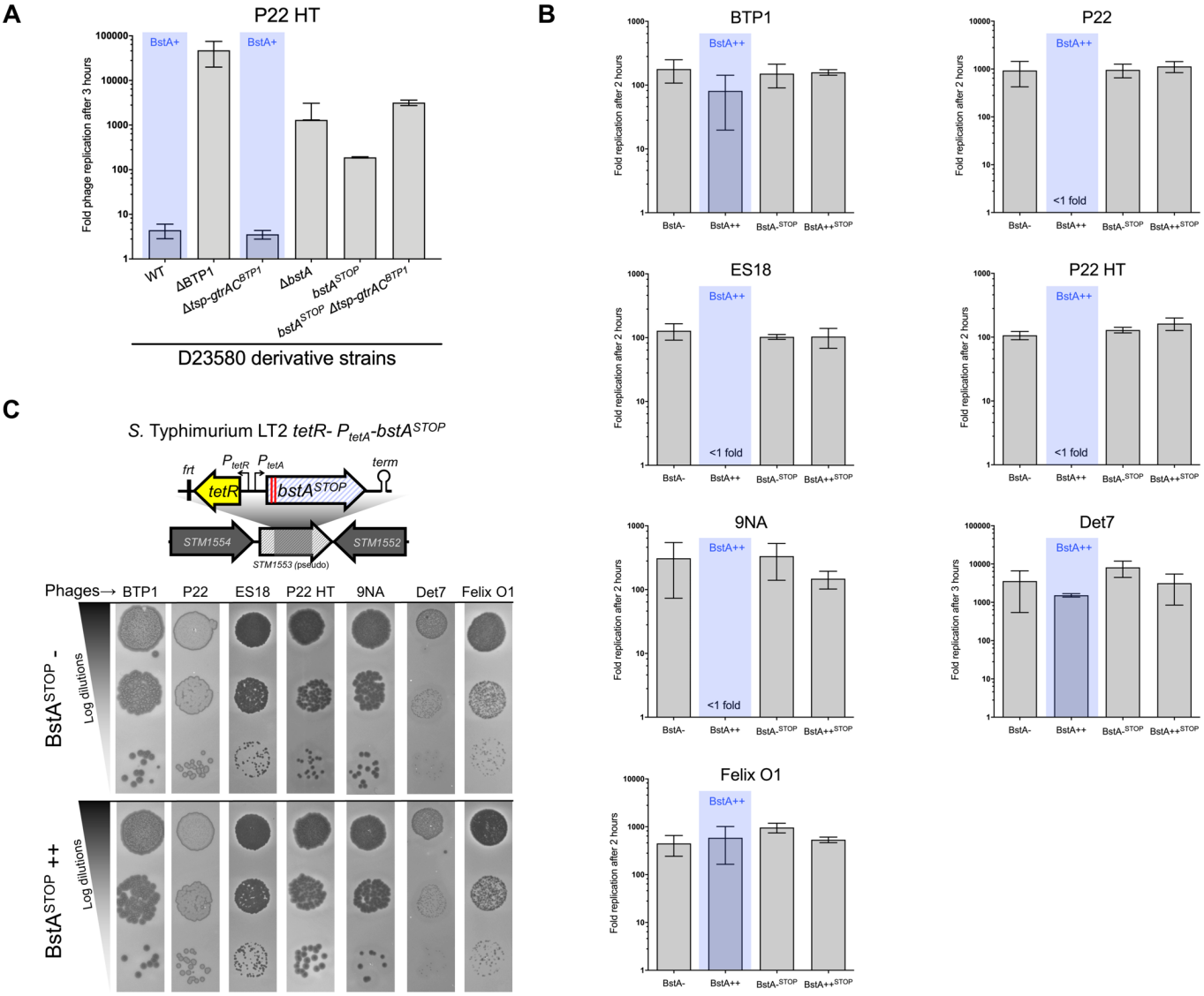

Supplementary Figure 1: The *bstA* locus confers phage resistance and *bstA* nonsense mutations supresses the phage resistance phenotype

(**A**) P22 HT (P22 HT *105/1 int-201*) replication assay on *S.* Typhimurium D23580 WT, or ΔBTP1, Δ*bstA*, *bstA*^{STOP}, Δ*tsp-gtrAC* and Δ*tsp-gtrAC bstA*^{STOP} mutants (strain JH3877, SSO-204, SSO-78, JH4287 and SNW431, respectively). Replication was measured 3 hours post-infection and phages were enumerated on lawns of D23580 Δ*tsp-gtrAC bstA*^{STOP} (SNW431). (**B**) Replication assays of the indicated phages were carried with mock-induced (BstA-) or AHT-induced (BstA++) strains LT2 *tetR-P*$_{tetA}$*-bstA*^{BTP1} (JH4400) or LT2 *tetR-P*$_{tetA}$*-bstA*^{STOP} (JH4402, carrying two nonsense mutations in *bstA*), as host. Phage replication was measured 2-3 hours post infection and phages were enumerated on lawns of LT2 WT. Phage replication (log_{10}-transformed folds) is presented as the mean of biological triplicates ± SD. ND = Replication not-detected. (**C**) Nonsense mutations in *bstA* suppress the BstA-driven anti-phage phenotype. Plaque assay were carried out with the indicated phages on mock- or AHT-induced lawns of LT2 *tetR-P*$_{tetA}$*-bstA*^{STOP} (JH4402).

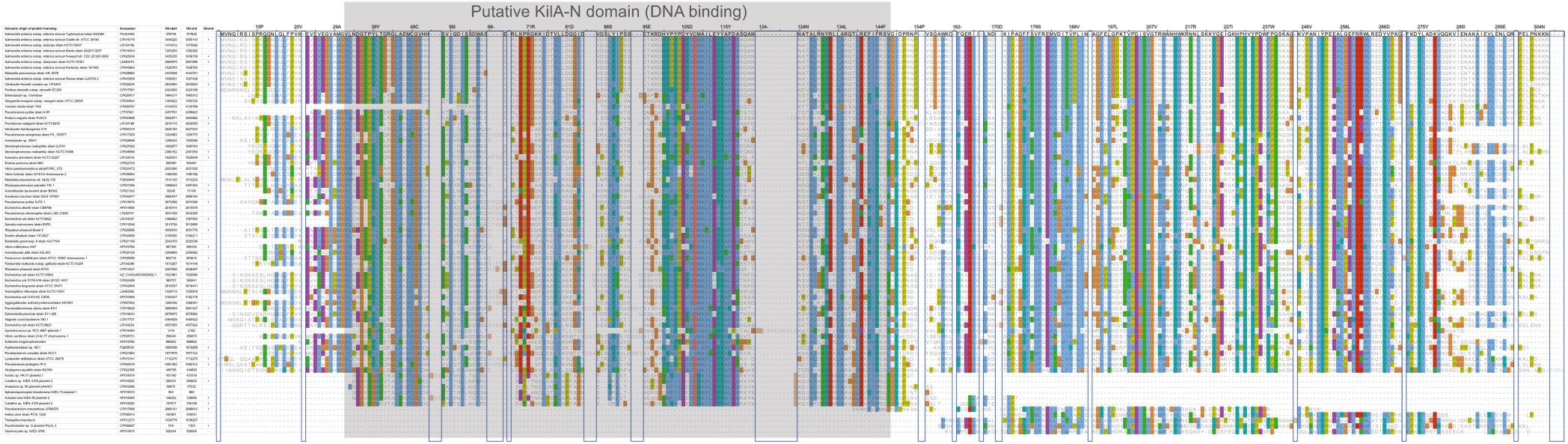

Supplementary Figure 2: Extended alignment of BstA protein homologs showing all columns and strain names
Blue boxes indicate columns which are gaps relative to the reference sequence (top row, BstA from *S.* Typhimurium D23580), and are collapsed in the alignment shown in Figure 2. Grey box indicates the position of the putative KilA-N domain.

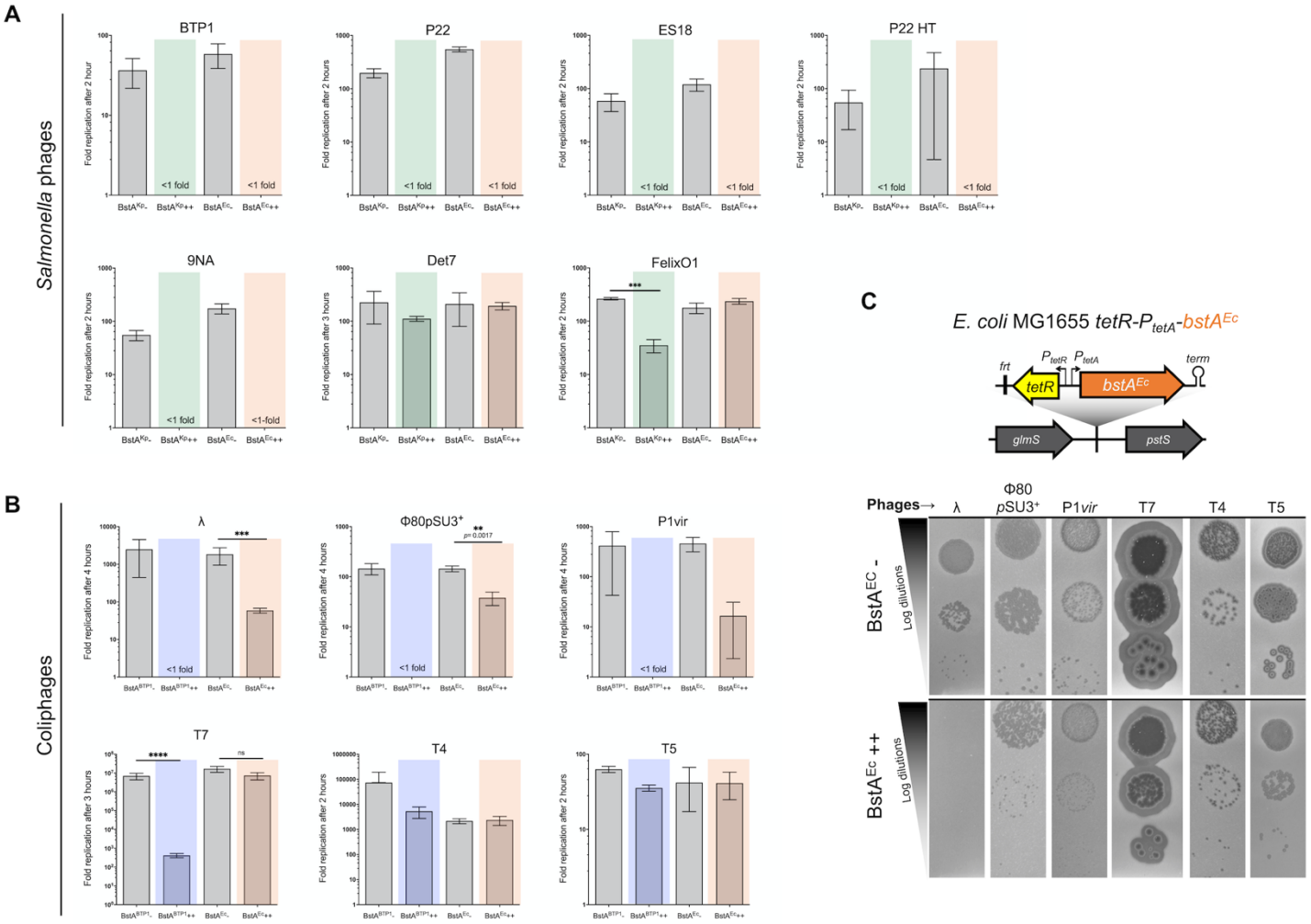

Supplementary Figure 3: BstA homologs confer phage resistance in *S.* Typhimurium LT2 and *E. coli* MG1655
(**A**) $BstA^{Kp}$ and $BstA^{Ec}$ confer phage resistance in *S.* Typhimurium. (**B**) $BstA^{BTP1}$ and $BstA^{Ec}$ confer phage resistance in *E. coli*. Phage replication assays were carried out with mock-induced (BstA-) or AHT-induced (BstA++) cultures of LT2 *tetR-P*$_{tetA}$*-bstA*^{Ec} (JH4408), LT2 *tetR-P*$_{tetA}$*-bstA*^{Kp} (JH4404), MG1655 *tetR-P*$_{tetA}$*-bstA*^{BTP1} (JH4410) or MG1655 *tetR-P*$_{tetA}$*-bstA*^{Ec} (JH4414), infected with the indicated phage. LT2 or MG1655 WT lawns were used for phage enumerate 2-3 hours post infection. Phage replication (log_{10}-transformed folds) is presented as the mean of biological triplicates ± SD. ND = Replication not-detected. When replication difference between induced and non-induced cultures was lower than one order of magnitude, groups were compared using unpaired two-tailed Student *t*-test and P values and significance are indicated by *,**,*** or ns (not significant). (**C**) $BstA^{Ec}$ confers phage resistance to *E. coli*. Plaque assay were carried out with the indicated phages applied on a lawn of mock- or AHT-induced MG1655 *tetR-P*$_{tetA}$*-bstA*^{Ec} (JH4414).

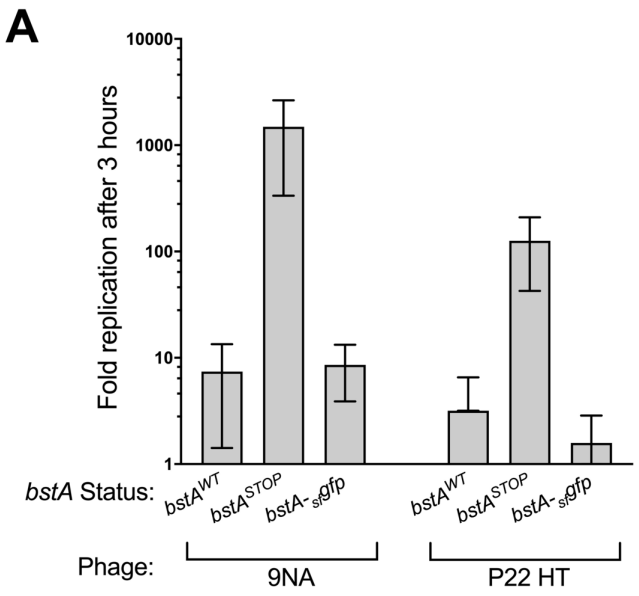

Supplementary Figure 4: C-terminal Superfolder GFP (sfGFP) fusion to BstA does not impair the BstA anti-phage activity

Replication assays were carried with the indicated phages on strains carrying the WT *bstA* (*bstA*^{WT}, strain D23580 in panel A, the defective *bstA*^{STOP} version (strain SSO-78) or the BstA-sfGFP fusion strain (*bstA-*$_{sf}$*gfp*, strain SNW403). Phage replication was measured 3 hours post-infection and plaques were enumerated on lawns of D23580 Δ*tsp-gtrAC bstA*^{STOP} (SNW431). Phage replication is presented on a $\log_{10}$ scale as the mean of biological triplicates ± SD.

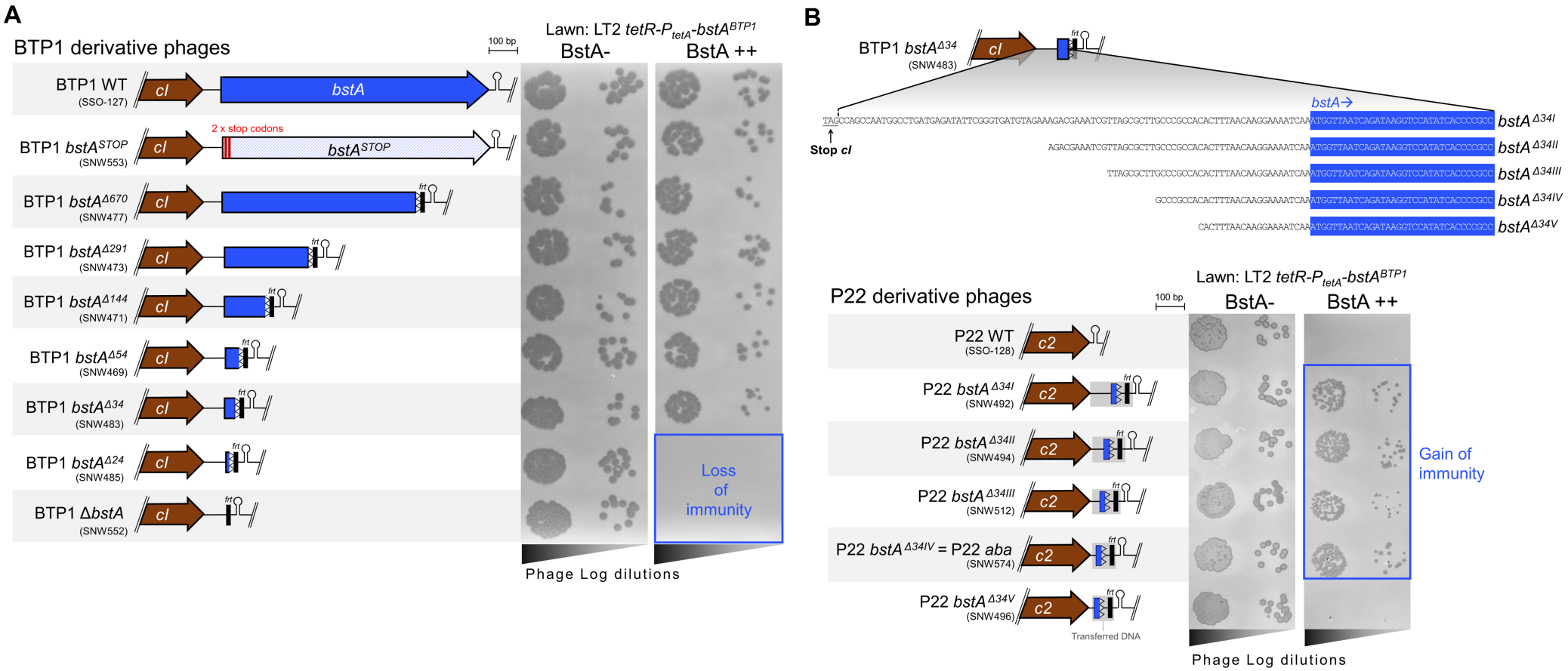

Supplementary Figure 5: Identification of the anti-BstA (*aba*) factor

(**A**) BTP1 *bstA* locus truncations revealed the location of the *anti-bstA* fragment *aba*. The *bstA* truncations are indicated for each BTP1 variant. The $bstA^{\Delta}$ allelic numbering corresponds to the number of base pairs remaining from the *bstA* ATG start. (**B**) Transfer of the $bstA^{\Delta 34}$ fragment in P22 confers BstA-immunity. Fragments $bstA^{\Delta 34I}$- $bstA^{\Delta 34V}$ are indicated. The donor strain for each BTP1 and P22 variant is indicated in brackets. The residual scar sequence of pKD4 is indicated by *frt* and hairpins represent rho-independent terminators. Plaque assays were performed with the indicated BTP1/P22-derived phages on lawns of mock-induced (BstA-) or AHT-induced (BstA++) LT2 $tetR\text{-}P_{tetA}\text{-}bstA^{BTP1}$ (JH4400).

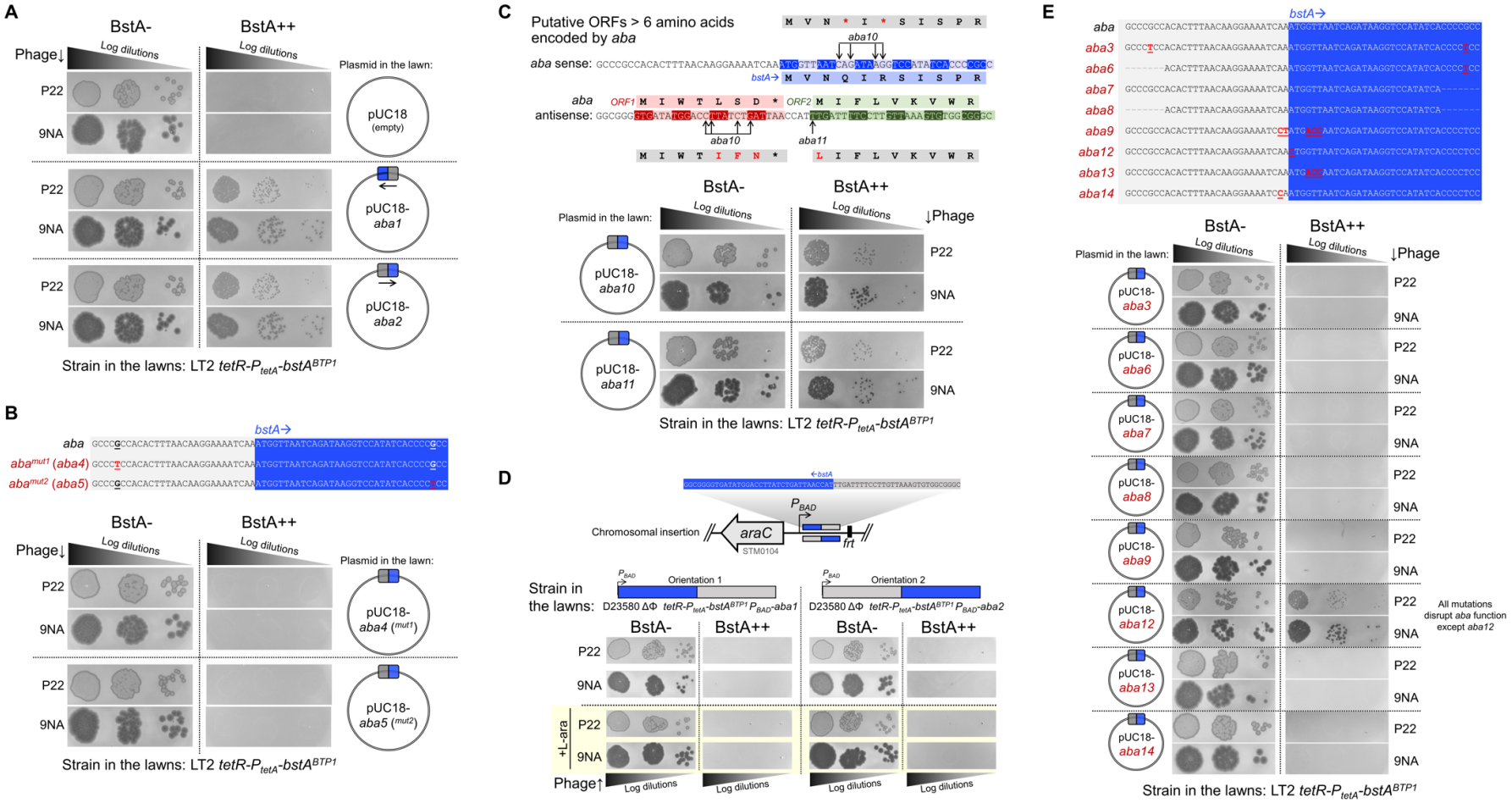

Supplementary Figure 6: Multiple copies of *aba* DNA suppresses BstA activity in *trans*

(**A**) The *aba* sequence was cloned into the pUC18 plasmid in either orientation, and the plasmids were transformed into LT2 *tetR-P*$_{tetA}$*-bstA*^{BTP1} (JH4400). Plaques assays were performed with phage P22 and 9NA applied on lawns of mock-induced (BstA-) or AHT-induced (BstA++) LT2 *tetR-P*$_{tetA}$*-bstA*^{BTP1} (JH4400), transformed with the indicated plasmid. Both plasmids (pUC18-*aba1* and pUC18-*aba2*) supressed BstA activity and permitted plaque formation by P22 and 9NA in the presence of BstA. (**B**) When a single nucleotide mutation was made in either of the terminal CCCGCC motifs, the pUC18 *aba* plasmids could not rescue the replication of P22 or 9NA in the presence of BstA. (**C**) Analysis of the *aba* sequence: putative open reading frames (ORFs) encoding for peptides longer that 6 amino acids are shown. All the ATG, TTG or GTG triplets were considered as putative start codons. The mutations of the functional *aba10* and *aba11* (shown in A) and the resulting mutated residues (in red) in the putative ORFs are indicated. Stop codons are indicated by *. Non-synonymous mutation in the putative ORFs does not disrupt *aba* suppression of BstA, therefore *aba* is unlikely to function via a peptide. (**D**) Transcription of *aba* does not counteract the BstA anti-phage activity. The *aba* sequence was inserted in both direction in the chromosome of strain D23580 ΔΦ *tetR-P*$_{tetA}$*-bstA*^{BTP1} (strains SNW618 and SNW619), downstream of the native arabinose-inducible promoter P_{BAD} (bended arrow) controlled by the AraC regulatory protein. Plaques assays were performed with the indicated phages and strains in the presence or absence of L-arabinose (0.2%). Induction of the transcription of *aba* by L-arabinose did not suppress the activity of BstA (P22 and 9NA phage plaquing is inhibited). (**E**) Further mutational disruption was made to the *aba* sequence cloned into pUC18 plasmids, to identify regions of the sequence that are essential for *aba* function. All mutations to pUC18 *aba* were non-functional (i.e. not capable of BstA suppression) except for the *aba12* derivative. Plaques assays were performed with phage P22 and 9NA applied on lawns of mock-induced (BstA-) or AHT-induced (BstA++) LT2 *tetR-P*$_{tetA}$*-bstA*^{BTP1} (JH4400), transformed with the indicated plasmid.